



Norwegian University of
Science and Technology

Monopile foundations

Effect of scour protection on eigenfrequency
of offshore wind turbines

Kjell Inge Sævdal

Geotechnics and Geohazards

Submission date: June 2017

Supervisor: Arnfinn Emdal, IBM

Norwegian University of Science and Technology
Department of Civil and Environmental Engineering



Report Title: Monopile Foundations Effect of scour protection on eigenfrequency of offshore wind turbines	Date: 07.06.2017 Number of pages (incl. appendices): 90
	Master Thesis <input checked="" type="checkbox"/> Project <input type="checkbox"/>
Name: Kjell Inge Sævdal	
Professor in charge/supervisor: Asst. prof. Arnfinn Emdal, NTNU	
Other external professional contacts/supervisors: Prof. Gudmund Eiksund, NTNU	

Abstract:

Monopile foundations is the most popular foundation type for offshore wind turbines, with over 80 % of the substructures being monopile foundations. When placed in a marine environment monopiles is prone to scour around the pile. This can influence the eigenfrequency of the wind turbine, which is a major design driver. To prevent scouring it is possible to place scour protection around the pile, normally consisting of a filter and armor layer.

The effect of scour protection has been investigated with a 3D-FEM analysis in Plaxis with a real size model with characteristic properties for a monopile pile placed in sand. Hardeing Soil Small (HSS) soil model has been used for the sand. The results from the simulations have been used to calculate p-y curves representing the soil response along the pile. Three different cases have been investigated, 1) a benchmark case without scour protection, 2) scour protection as surface load and 3) a full scour protection layer. The lateral load on the monopile were divided into 5 load steps, 10 kN, 100 kN, 1000 kN, 2000 kN and 5000 kN. Also, a simple 1-DOF approximation has been used to compare the eigenfrequencies of the three cases.

The results from the simulations show a 1 % increase in eigenfrequency for the case with surface load at load step 100 kN and the case with a full scour protection layer show 10 % increase in eigenfrequency. Also, a comparison with DNV/API design codes for p-y curves have been done for the benchmark case, giving a good match for shallow depths, but for larger depths the DNV/API formulations give higher stiffness. This is mainly due to the linear increase in stiffness with depth in the DNV/API formulations where HSS have parabolic increase with dept.

Keywords:

Monopile

Scour protection

Eigenfrequency

Kjell Inge Sævdal

MASTERS DEGREE THESIS

Spring 2017

Kjell Inge Sævdal

Monopile Foundations

Effect of scour protection on eigenfrequency of offshore wind turbines

BACKGROUND

Offshore wind energy has become a large supplier of green energy to the European energy market, with more than 3.200 offshore wind turbines installed. The trend in the offshore wind industry is towards bigger turbine size, deeper-seated turbines and increased focus on cost optimization. The monopile foundation is the most common foundation type with over 80 % of the installed wind turbines using monopile foundations. When a structure is placed in marine environment it is prone to erosion of the seabed materials surrounding the structure, so called scour. This can affect the lateral response of the structure. To prevent scouring, a scour protection is placed around the structure, usually a filter and armour-layer consisting of medium and coarse sized rocks.

TASK

The objective of the thesis is to evaluate the effect of the scour protection on the eigenfrequency of offshore wind turbines. The static lateral soil response of a monopile shall be studied by use of the 3D-FE analysis program Plaxis 3D. A full-scale model with the Hardening Soil Small (HSS) soil model shall be used. The simulations should consider a benchmark case without scour protection, a case with only surface load and a case with a full scour protection layer. The resulting soil response from the simulations should be used to calculate p-y curves along the pile and the results should be compared with design codes by DNV/API. Also, the eigenfrequency for the different cases should be calculated and compared using a simple 1-DOF approximation.

Task description – thesis structure

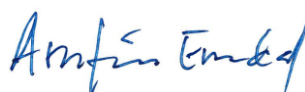
- Background and motivation for the topic
- An introduction to design of monopile foundations for offshore wind turbines
- Presentation of the 3D-FE model used and a method for extracting soil response
- Presentation of the results from the simulations
- Comparison with DNV/API formulations for p-y curves
- Comparison of eigenfrequencies for the different cases

Professor in charge: Asst. prof. Arnfinn Emdal

Co-supervisor: Professor Gudmund Eiksund

Department of Civil and Transport Engineering, NTNU

Date: 06.06.2017



Arnfinn Emdal

This Master's thesis is dedicated to my grandfather Kjell who passed away during this semester. Thank you for encouraging make the most of every opportunity and take on every adventure. You will forever live in our harts.

Preface

This is a master's thesis in geotechnics at NTNU as part of the MSc in Geotechnics and Geohazards, it was carried out during the spring semester of 2017. The idea for this project was brought up by the geotechnical group at NTNU.

The topic of this master's thesis is monopile foundations for offshore wind turbines. The aim of this project is to quantify the effect of the scour protection on the eigenfrequency of offshore wind turbines by conduction simulations with 3D finite element (FEM) software Plaxis to evaluate the lateral response of the soil and scour protection layer. The results from the simulations have been used to calculate p-y curves and compare them with current design codes like those given by DNV GL and American Petroleum Institute (API). The change in eigenfrequency have also been investigated.

Trondheim, 2017-06-07



Kjell Inge Sævdal

Acknowledgement

I would like to thank the following persons for their great help during this master's thesis. Professor *Gudmund Eiksund* for his guidance in the field of offshore wind turbines and monopile foundations, and for his ideas and contribution to the problem formulation for this master project. He has also been most helpful with calculation principles and methods for extracting p-y curves from Plaxis. My supervisor associate professor *Arnfinn Emdal* for his guidance and support during this project and for many good discussions.

Kjell Inge Sævdal

Summary and Conclusions

Offshore wind energy i.e. offshore wind turbines have become a large supplier of clean renewable energy to the European energy market. By the end of 2015 it was installed over 3.200 offshore wind turbines in 84 offshore wind farms in 11 European countries, delivering over 11.000 MW of clean renewable energy to the grid. For offshore wind turbines 80 % of the substructures are monopiles.

The main principle for designing offshore wind turbines with monopile foundation is to fit the natural frequency of the structure within a section of frequencies that is not interfering with the natural frequencies from wind, waves and the rotor and blade passing frequencies. This is done by modelling the pile as beam element with non linear springs, an so called *Winkler foundation* with p - y springs. These springs simulate the response of the soil.

The development of the natural frequency of the offshore wind turbine is also dependent of the bed condition over time. When a structure is placed in a marine environment the flow around the structure changes. The structure represents an obstacle that the current or waves (also combined wave and current) have to pass. The presence of the structure can induce wakes and vortexes that increase the shear stress on the bed surface, and when the shear stress is higher than the shear strength ($\tau > \tau_f$) erosion of bed material will start around the pile (scouring).

Scour can have a substantial impact on the natural frequency of an offshore wind turbine, and with frequency reduction comes possibility of resonance with other prominent dynamic loads on the structure, this can lead to increased fatigue, shorter operational lifetime and in worst case total breakdown of the structure. To protect a structure from the possibility of scour it is normal to place scour protection around it. The scour protection normally consists of a filter and armour layer consisting of medium and coarse sized stones.

The effect of scour protection on the lateral stiffness of monopiles for offshore wind turbines has been investigated through 3D-FEM analysis in Plaxis. The results from the simulations were used to calculate p - y curves for different depths and situations. The results were also compared to the American Petroleum Institute recommended and DNV GL recommended practice for calculating p - y curves for offshore purposes.

The 3D-FEM calculations were done with a model representing a real situation, with real sizes and parameters. The pile was 60 m long with a diameter of 6 m. The pile was embedded 30 m in sand. The sand selected was *Hokksund* sand, a model sand used at NTNU for laboratory tests. The FEM simulations was divided into three cases, 1) benchmark case without scour protection, 2) scour protection as surface load and 3) scour protection as a independent layer on top of the subsoil. Within these three cases the lateral load was divided in to 5 load steps, 10 kN, 100 kN, 1000 kN, 2000 kN and 5000 kN. The intervals of the load were chosen to give values from both small and larger loads to be able to evaluate the development of the p - y curves.

The results from the 3D-FEM simulations show a clear effect of both the surcharge load of the scour protection and the extra layer that the scour represents. The p - y curves from the Plaxis simulations fit well with the p - y curves from the API formulation down to about -3,12

m for the benchmark case, but with larger depths the API formulation predicts higher stiffness than what is observed in the simulations. This is in accordance with findings by among others Hanssen (2016). The frequency for the case with only surcharge load is found to be up to 1 % higher for load step of 100 kN than for the benchmark case. For the case with scour protection as a independent layer the frequency was found to be 10 % higher than the benchmark case. This indicates that the scour protection has a substantial impact in the eigenfrequency of a offshore wind turbine, and most impact has the stiff extra layer that the scour protection represents.

The conclusion to this master's project is that the design codes used in the industry for estimating the soil response do not adequately embrace the effect the scour protection has on the lateral behaviour of a monopile foundation. An effect of up to 10 % increase in eigenfrequency is observed when the SP is fully included in the numerical simulations. Both the surcharge component of the SP and the extra layer has an effect on the eigenfrequency.

Contents

- Preface iii
- Acknowledgements v
- Summary and Conclusions vii

- Nomenclature xv**

- 1 Introduction 2**

 - 1.1 Background 2
 - 1.1.1 Problem Formulation 4
 - 1.1.2 Literature Survey 4
 - 1.2 Objectives 4
 - 1.3 Limitations 5
 - 1.4 Approach 5
 - 1.5 Structure of the Report 6

- 2 Design of Monopile Foundation 7**

 - 2.1 Design principles 7
 - 2.1.1 Loads 8
 - 2.2 Design Criteria for Monopile Foundations 10
 - 2.3 Scour Around Large Diameter Monopiles 11
 - 2.3.1 Development of scour 11
 - 2.3.2 Scour around a single slender pile 11
 - 2.3.3 Calculation of scour depth 14
 - 2.4 Theoretical Background for Foundation Design 15
 - 2.4.1 Formulation of p-y curves 15
 - 2.4.2 Modification of p-y curve formulation 22
 - 2.5 Effect of Cyclic Loading on Lateral Response 23

- 3 Model Used in Simulations 27**

 - 3.1 Hardening Soil Small Soil Model 27
 - 3.2 Soil properties 27
 - 3.2.1 Linear Elastic Soil with Stiffness from Oedometer Testing 28
 - 3.2.2 HSS with Stiffness from SWV and Oedometer 29
 - 3.3 3D-FEM model in Plaxis 32
 - 3.3.1 Pile Geometry 32
 - 3.3.2 Properties of Scour Protection Layer 33
 - 3.3.3 Load characteristics 33
 - 3.4 Simulation Staging in Plaxis 34
 - 3.4.1 Benchmark Study Without Scour Protection 35
 - 3.4.2 Scour Protection as Surface Load 35
 - 3.4.3 Scour Protection as Dedicated Layer 35

4	Results from Simulations	36
4.1	Bending Moment and Soil Response from Simulations	36
4.1.1	Results from Case Without Scour Protection	39
4.1.2	Results from Case With Surface Load	42
4.1.3	Results from Case With Scour Protection Layer	45
4.2	Lateral Deflection from Simulations	48
4.3	Calculation of p-y curves from Simulations	49
5	Discussion	52
5.1	Comparison of Results	52
5.1.1	Change in p-y Curves	52
5.2	Change in Eigenfrequency	54
5.2.1	Stiffness of Scour Protection Layer	58
6	Summary and Conclusion	60
6.1	Recommendations for Further Work	63
	Bibliography	64
A	Determination of HSS Parameters for Hokksund Sand	

List of Figures

- 1.1 Foundation design principles for offshore wind turbines 3
- 2.1 Example of dimensions and forces acting on a wind turbine 8
- 2.2 Overview of frequencies for a 3,5 MW turbine with 5-13 rpm operational interval 9
- 2.3 Development of horseshoe and Lee-wake vortexes around a pile 12
- 2.4 Stress distribution in a laterally loaded pile 16
- 2.5 Concept of soil response curves for a laterally loaded pile 16
- 2.6 Short term static loading 18
- 2.7 Short term dynamic loading 19
- 2.8 Graphs to determine the c and k coefficients 21
- 2.9 Strain wedge in uniform soil 24
- 2.10 Pile deflection curves for 3 cyclic lateral loads 25

- 3.1 Characteristic stiffness-strain behaviour of soil with typical strain rages for structures and laboratory tests 28
- 3.2 Change in E_s with depth according to eq. 3.2. 29
- 3.3 Measured shear wave velocity and calculated small strain modulus against vertical stress 30
- 3.4 Small strain modulus G_{max} with depth 31
- 3.5 Model from Plaxis with scour protection layer. 32
- 3.6 Change in G_0 , $G_{0,HS}$, $G_{0,HSSP}$ and γ_{07} with depth down to 40 m for the scour protection layer. 34

- 4.1 Derivatives of the 4th order beam equation 37
- 4.2 Flow chart of calculation procedure for p-y curves from Plaxis. 37
- 4.3 Model from Plaxis with no scour protection and load of 5000 kN. 39
- 4.4 Moment and soil response with depth for case with no scour protection. . . . 40
- 4.5 Moment distribution from Plaxis along beam for case without scour protection at load step 5000 kN 41
- 4.6 Interface stress for case without scour protection at load step 5000 kN. 41
- 4.7 Model from Plaxis with surface load and load of 5000 kN. 42
- 4.8 Moment and soil response with depth for case with surface load. 43
- 4.9 Moment distribution from Plaxis along beam for case with surface load at load step 5000 kN 44
- 4.10 Interface stress for case with surface load at load step 5000 kN. 44
- 4.11 Model from Plaxis with scour protection layer and load of 5000 kN. 45
- 4.12 Moment and soil response with depth for case with scour protection layer. . . 46
- 4.13 Moment distribution from Plaxis along beam for case with scour protection at load step 5000 kN 47
- 4.14 Interface stress for case with scour protection layer at load step 5000 kN. . . . 47
- 4.15 Pile deflection at 5000 kN for all cases. 48

4.16	p-y curves from -0,61 to -14,4 m.	49
4.16	p-y curves from -0,61 to -14,4 m cont.	50
4.17	p-y curves from -23,1 to -26,7 m.	51
5.1	Moment and soil response with depth for a load of 5000 kN for all cases.	53
5.2	p-y curves based on API formulation for case without scour protection.	54
5.3	p-y curves based on API formulation (bold text) for case without scour protection compared with p-y curves from Plaxis.	55
5.4	p-y curves in the small strain area based on API formulation (bold text) for case without scour protection compared with p-y curves from Plaxis.	55
5.5	Change in eigenfrequency for a pile with mass on top.	57
5.6	Deformation of scour protection layer with horizontal load of 5000 kN.	58
5.7	p-y curve for SP layer at 0,66 m.	59

List of Tables

- 1.1 Overview of European offshore wind industry 2
- 2.1 Partial factors for ULS and SLS 10
- 2.2 Mobilised lateral resistance - displacement for short-term static loading 18
- 2.3 Mobilised lateral resistance - displacement for short-term cyclic loading 19
- 2.4 Rate of increase with depth of initial modulus of subgrade reaction 21
- 2.5 Diameter exponent for varying displacement 22

- 3.1 Key soil parameters of Hokksund sand 28
- 3.2 Parameters for the HSS model 31
- 3.3 Pile properties 33
- 3.4 Parameters for the HSS model of the scour protection layer 34

- 5.1 Data used to calculate the frequency for all cases and load steps. 56

Nomenclature

α	stress exponent
$\Delta\sigma_h$	variation in horizontal force in the wedge face
ϵ_C	strain at 0,5 of maximum deviatoric stress in uniaxial compression test
γ'	submerged unit weight of the soil
ν	Possion's ratio
ϕ	friction angle of material
ϕ_m	mobilised friction angle of the soil
ρ	density [kg/m^3]
σ'_v	effective vertical stress
σ_a	reference stress 100 kPa
τ	shear stress at pile side
θ	Shields parameter
θ_{cr}	critical Shields parameter
c_1, c_2, c_3	factors depending on the internal friction angle of the sand
c_u	undrained shear strength
D_0	reference diameter (0,61m)
E^*	equivalent Young's modulus
E_o^{py}	initial soil stiffness
E_s	Young's modulus
G_s	small strain modulus
$G_{s,max}$	shear modulus at small strains
K_0	earth pressure coefficient at rest

k_s	force/displacement at top of pile
M_s	constraints modulus of the soil
p'_0	effective overburden stress at depth
p_r	representative lateral capacity in units force per unit length
p_u	modified ultimate resistance
U_{max}	maximum orbital velocity at the bed
v_s	shear wave velocity [m/s]
X_R	depth below sea floor to the bottom of reduced resistance zone
z_0	reference depth
c	cohesion
D	diameter of pile
g	acceleration on gravity
H	wave height
h	height of passive wedge
h	water depth
I	2^{nd} area moment of pile
J	dimensionless parameter
k	initial modulus for sub-grade reaction
k	wave number
KC	Keulegan-Carpenter number
M	moment from Plaxis
M	top mass
m	diameter exponent
m	modulus number
n	site specific parameter 0,4-0,7
p	mobilised lateral resistance in unit force per unit length
r	radius
S	scour depth
T	wave period

t	thickness of pile walls
X	depth below sea floor
y	local lateral displacement
z	depth

Introduction

Offshore wind energy, primarily offshore wind turbines, have become a large supplier of clean renewable energy to the European energy market. By the end of 2015 it was installed over 3.200 offshore wind turbines in 84 offshore wind farms in 11 European countries, delivering over 11.000 MW of energy to the grid.

1.1 Background

Table 1.1: Overview of European offshore wind industry, EWEA (2015, 2014)

	2015	2014
New number of turbines	419	408
Total number of turbines	3230	2488
Average output	4,2 MW	3,7 MW
Combined output	11027 MW	8045 MW
Average water depth	27,1 m	22,4 m
Average distance to shore	43,3 km	32,9 km
Monopile foundation	80 %	78,8 %

Monopiles is the most common foundation type where around 80 % of the substructures are monopiles. The average turbine size is 4,2 MW, the average water depth is 27,1 m and the average distance from shore is 43,3 km. The trend is an increasing turbine size (14 % larger from 2014 to 2015) and even bigger water depths and distance from shore, see table 1.1.

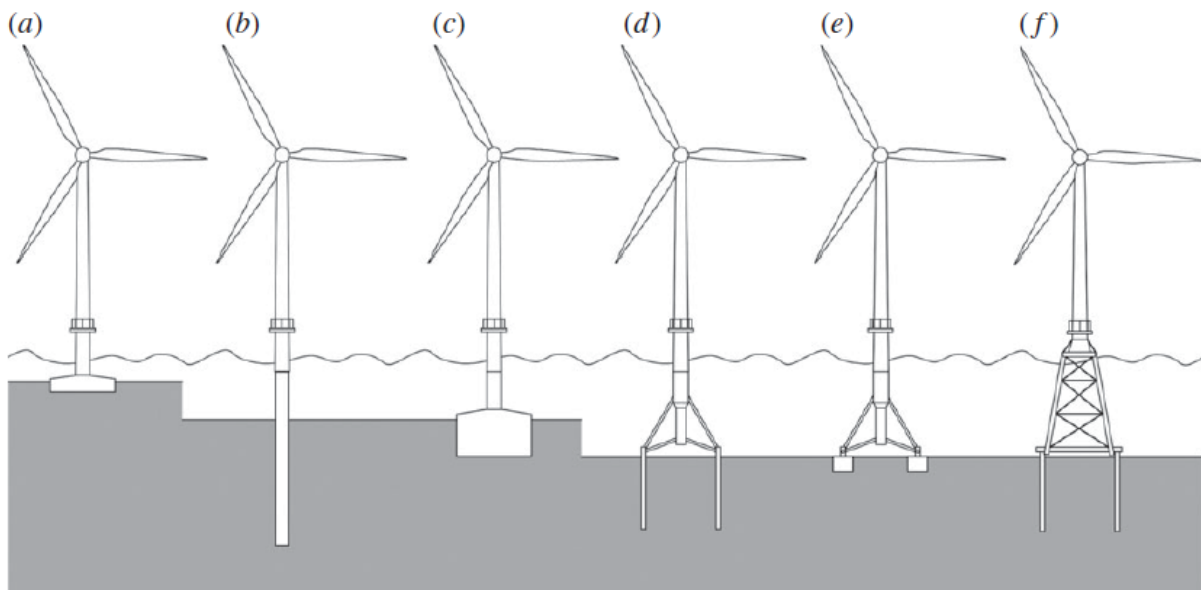


Figure 1.1: Foundation design principles for offshore wind turbines, from Kallehave (2015).

Design of support structure depends on in-situ conditions, specially water depth can be a limiting factor when deciding what type of support structure (foundation) is feasible. There are many different foundation types (principles) for offshore wind turbines, see figure 1.1:

- (a) Gravity based foundation
- (b) Monopile foundation
- (c) Cassion foundation
- (d) Multiple foundation
- (e) Multiple cassion foundation
- (f) Jacket foundation

These different foundation designs have different advantages and disadvantages, but the monopile foundation has proven to be the most versatile and cost effective solution. With the increasing demand for renewable energy, the industry is continuously striving to reduce manufacturing and operational cost. The trend is towards bigger and deeper seated turbines. This effort has resulted in optimisation of support structure and foundation design. Today there is plans to install 6-8 MW turbines in water depths of 20-40 m on large monopiles up to 7,5 m in diameter. Monopiles is also suitable for mass production and standardisation, which illustrates that monopiles also in the future will be the preferred support structure for offshore wind turbines (Kallehave, 2015b).

Scour protection

When a structure is placed in a marine environment it is prone to scour (erosion of bed sediments around the structure) caused by the increased shear stress on the seabed due to change in flow around the structure. The main design criterion of a offshore wind turbine is the eigenfrequency (natural frequency). This is to prevent resonance with wind, wave and rotor excitation frequencies which the structure is exposed to. To prevent scour it is common to place scour protection around the structure. The scour protection normally consists of a

filter- and armour layer. Just as scour, the scour protection can influence the eigenfrequency of the structure. The extra layer acts as a surcharge on the subsoil, and the scour protection (rocks) also have a high lateral stiffness when it is in contact with the monopile. This will change the dynamic response of the monopile foundation, and ultimately the dynamic response of the whole structure.

1.1.1 Problem Formulation

As described earlier the monopile foundations is widely used in the offshore wind industry as foundations for offshore wind turbines. The dynamic response of the structure is very much governed by the interaction between the monopile and the surrounding soil. The soil response is in most cases modelled as springs along the structure (Winkler foundation) with varying stiffness, this gives an opportunity to calculate the dynamic response for many load combinations. The soil response is stress dependent, i.e. the soil gets stiffer in higher stress situation.

In some areas, the monopile foundation is exposed to scour (erosion of material around the structure). This can have an impact on the eigenfrequency of the structure. To prevent this from occurring it is possible to place scour protection around the structure, normally consisting of a filter layer (small rocks) and an armour layer (rocks). The scour protection will act as an surcharge load on the surface of the soil surrounding the structure, and as an extra layer with lateral stiffness acting on the structure. This will lead to a stiffening of the subsoil caused by the extra vertical stress and an increased lateral stiffness around the monopile caused by the extra layer of rocks.

The aim of this project is to quantify the effect of the scour protection on the lateral response of an offshore wind turbine, to tell more what effect the scour protection have on the eigenfrequency of a offshore wind turbine. The main approach to solving this problem will be to conduct a 3D simulation in finite element (FE) software Plaxis with a real size model. The simulations will be divided in to three cases: no scour protection, surface load and scour protection layer.

1.1.2 Literature Survey

This master's thesis is based upon a project thesis done in the fall of 2016, which was a literature study on scour and scour protection around monopiles. Most of the background material used in this master's thesis is from this project.

1.2 Objectives

The objectives of this master's thesis is to:

- Review design procedures for offshore wind turbines with monopile foundation based on design codes.
- Present a method for using FEM software for estimating soil response.
- Evaluate the effect of scour protection on the lateral response of offshore wind turbines.

Questions that need to be answered:

- What is the main design approaches for design of offshore wind turbines with monopile foundations?
- Does the scour protection effect the lateral response of a offshore wind turbine?
- If so, what is the main contribution to this effect, the surcharge load or the scour protection layer?

1.3 Limitations

This project only considers the monopile foundation for offshore wind turbines. There is multiple other foundation types (see figure 1.1). There is multiple improved formulas (approaches) to evaluate the lateral response of the soil. This thesis only considers the procedures describes in design codes by DNV (2014); API (2011). The model used in the simulations is based on installed structures described in Kallehave (2015), and the soil model is similar to the model sand used at NTNU with Hardening Soil Small properties calculated from shear wave velocity measurements done by Hanssen (2016) and soil test described in Sandven (1992). The model used in the simulations represent half of a pile with symmetry boundary conditions in Plaxis. The results from the simulations is then valid for half of a pile. When comparing the p-y curve from the Plaxis simulations with DNV/API formulations the results is adjusted to represent a full pile. This is because DNV/API formulations gives p-y curves for a full pile.

1.4 Approach

The approach of this thesis has been to:

1. Establish a theoretical background for design of substructures for offshore wind turbines based on formulations by DNV (2014); API (2011) and the use of p-y curves to calculate the soil response and eigenfrequency of offshore wind turbines with monopile foundations.
2. Gather relevant properties of the soil and scour protection layer to be used in subsequent simulations.
3. Simulate the monopile foundation without any scour protection to establish a benchmark for comparison with subsequent simulations.
4. Simulate the monopile foundation with a realistic surface load to evaluate the effect of the scour protection on the stiffness and response of the sub-soil.
5. Simulate the monopile foundation with an scour protection layer with realistic unit weight and high lateral stiffness.
6. Use results from the simulations to calculate p-y curves along the monopile for the different cases to evaluate the change in soil response and eigenfrequency for the different cases.
7. Use the results from the simulations to compare the findings with results given by design codes by DNV (2014); API (2011).

1.5 Structure of the Report

This report is divided in to 6 chapters:

Introduction

This chapter presents the background for this project with some introduction to offshore wind statistics and a brief overview of the monopile design. This chapter also outlines the framework for this project.

Design of monopile foundations for offshore wind turbines

This chapter presents the basic design principles for monopiles for offshore wind turbines with reference to relevant design codes and recent research in this area. The theoretical background for the simulations is also described here. Also research on the effect of cyclic loading on the lateral response of offshore wind turbines is presented.

Model used in simulations

This chapter describes the model used in the simulations with the different cases.

Results from simulations

This chapter presents the results from the simulations.

Discussion

This chapter discusses the results from the simulations and compares the results for the different cases. Also a comparison with design codes by DNV (2014); API (2011) are presented here.

Conclusion, Summary and Recommendations for Further Work

This chapter summarise the results from the simulations and present a conclusion regarding the effect of scour protection on the lateral response in relation to the objectives outlined in this chapter. This chapter also present suggestions for further work.

Design of Monopile Foundation

This chapter is an introduction to the design principles of monopile foundations for offshore wind turbines and principles for scour protection. This chapter is the theoretical background for the simulations described in chapter 3. The main design approaches for offshore wind turbines is described in DNV (2014); API (2011) which is guidelines and design coded for design of offshore wind structures. This is the most common guidelines used in the world. Recent research done by Kallehave (2015); Hanssen (2016) concludes that the current design approaches and industry standards does not fully capture the soil behaviour, and consequently the structure is in most cases over-designed, i.e. "bigger" than it needs to be or the factor of safety is bigger than required. Considering the industry wide search for cost reduction this concludes that there is room for a more efficient design of the structure with resulting cost reductions.

2.1 Design principles

Structures and structural elements shall be designed to (DNV, 2014):

- Sustain loads liable to occur during all temporary, operating and damaged conditions if required.
- Ensure acceptable safety of the structure during the design life of the structure.
- Maintain acceptable safety for personnel and environment.
- Have adequate durability against deterioration during design life of the structure.

When designed all the parts of the structural system shall as far as possible satisfy the following requirements:

- Resistance against relevant mechanical, physical and chemical deterioration.
- Fabrication and construction complies with relevant, recognised techniques and practises.
- Inspection, maintenance and repair is possible.

To achieve this goals and requirements DNV (2014) incorporates *Limit States* for the design of the structure. The following limit states is described in the guideline:

- *Ultimate Limit State* (ULS) which is the maximum load carrying resistance.
- *Fatigue Limit State* (FLS) which represents failure due to the effect of load cycling.
- *Accidental Limit State* (ALS) which is (1) maximum load carrying capacity for (rare) accidental loads or (2) post-accidental integrity of damaged structure.
- *Serviceability Limit State* (SLS) which is the tolerance criteria for normal use.

DNV (2014) uses the *partial safety factor format* to obtain the target safety level. This is done by implementing load and resistance factors to characteristic values of the governing variables. The partial factor method is widely used in all geotechnical engineering and is also implemented in *Eurocode*.

2.1.1 Loads

Offshore wind turbine is exposed to dynamic loads in form of wind load, wave load and rotor excitation (blade passing the tower and instability in the rotor). These loads have different frequencies and amplitudes which interacts with the overall structure. To prevent amplification of the structural response of the structure, the design is optimised to allow the natural frequency of the structure to be between the excitation frequencies and the blade passing frequency.

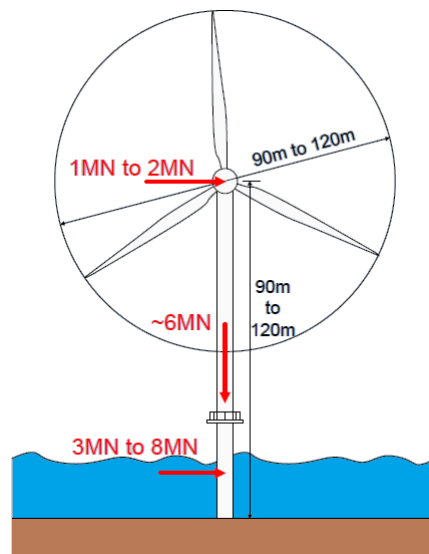


Figure 2.1: Example of dimensions and forces action on a wind turbine, from Byrne (2011).

Lombardi et al. (2013) divide the loading conditions on a wind turbine in to three categories:

- Environmental dynamic loads from wind and waves.
- Rotor loading frequency ($1P$) generated from instability in the rotor.
- Blade passing frequency ($3P$) generated from the wind deficiency when a blade passes through the shadow of the tower.

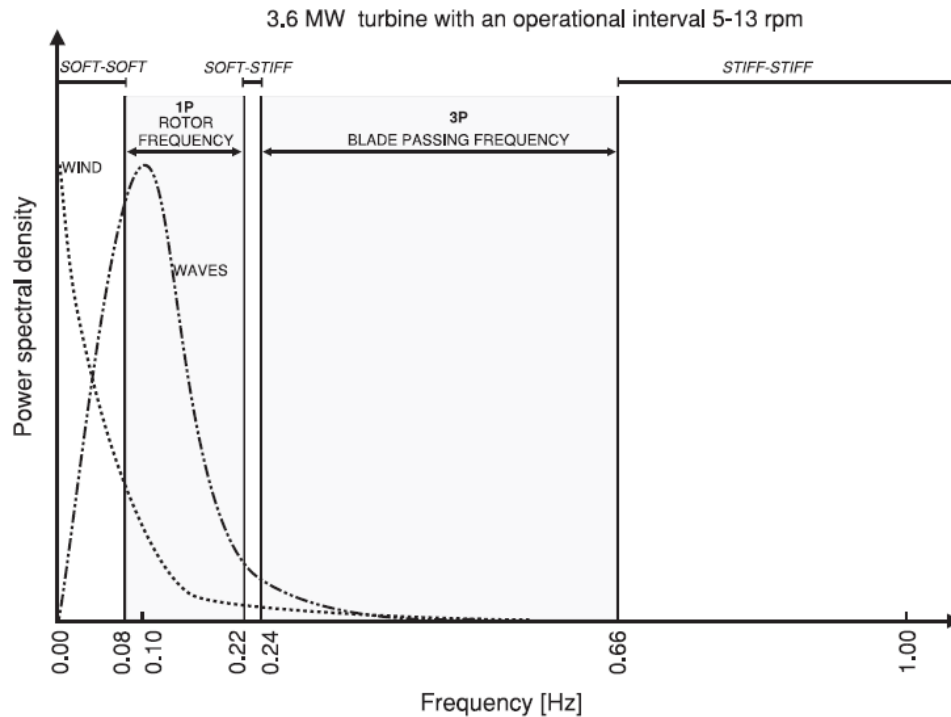


Figure 2.2: Overview of frequencies for a 3,5 MW turbine with 5-13 rpm operational interval, from Lombardi et al. (2013).

When considering the design codes, DNV (2014) recommends that the natural frequency of the structure is at least $\pm 10\%$ away from the 1P and 3P frequencies. When considering these recommendation Lombardi et al. (2013) defines three different design approaches:

- soft-soft where the natural frequency is lower that the rotor loading frequency, $f_0 < 1P$, where f_0 is the natural frequency if the system.
- soft-stiff where the natural frequency is between the rotor loading frequency and the blade passing frequency, $1P < f_0 < 3P$.
- stiff-stiff where the the natural frequency is higher than the blade passing frequency, $f_0 > 3P$.

The most common design approach is the soft-stiff approach, likely due to the fact that a stiffer design will need stiffer elements i.a more materials used and a softer design will be close to the frequency of the environmental loads. In figure 2.2 the frequency spectrum for a 3,5 MW turbine is shown.

DNV (2014) states that the geotechnical design of the foundation shall consider both the strength and deformation of the foundation and the foundation soil. The failure modes of a foundation might be:

- Bearing failure
- Sliding
- Overturning

- Pile pull-out
- Large settlement or displacements

2.2 Design Criteria for Monopile Foundations

According to DNV (2014) both ultimate limit state (ULS) and serviceability limit state (SLS) shall be considered when designing monopile foundations for offshore wind turbines. The strength and deformation properties of the pile as well as the soil shall be the basis of the load-carrying calculations. The evaluation of soil resistance against the loads from the pile should consider the following factors:

- Shear strength characteristics
- Deformation properties and in-situ stress conditions of the foundation soils
- Method of installation
- Geometry and dimension of the pile
- Type of loads

For monopile foundations the data base of existing methods for calculation of soil resistance to axial and lateral pile loads are often not covering all conditions relevant for offshore piles. DNV (2014) states that when determining the soil resistance to said pile loads extrapolation between the data base of a chosen method shall be made with evaluation of all parameters involved. It is also stated that the selected foundation method is feasible with respect to installation of the pile, and that the stability of the whole structure shall be assessed with respect to stability for both operation and temporary design conditions.

For calculating the ULS and SLS the following material parameters shall be considered unless otherwise is specified:

Type of geotechnical analysis	ULS γ_m	SLS γ_m
Effective stress analysis	1.15	1.0
Total stress analysis	1.25	1.0

Table 2.1: Partial factors for ULS and SLS, from DNV (2014).

For laterally loaded piles the ULS may be based on theory of plasticity based on the assumption that the lateral displacement of the pile is sufficient to plastify the soil completely. The characteristic resistance in the soil shall be in accordance with recognised plastic theorems to avoid non-conservative estimates. When analysing piles stress and pile head displacements DNV (2014) states that the lateral resistance shall be modelled using characteristic soil strength parameters with material factor equal to $\gamma_m = 1,0$. Also the non-linear response of the soil and effects of cyclic loading shall be accounted for.

2.3 Scour Around Large Diameter Monopiles

Generally offshore structures connected to the seabed is exposed to scour around the structure due to change in the velocity in the water stream around the structure. Scour can have an dramatic effect on the structure, and can lead to loss of bearing capacity, fixity and/or stiffness. Offshore wind turbines are sensitive to change in stiffness because of it's design.

2.3.1 Development of scour

Scour is the name for erosion of sediment around a structure. The interaction between the structure and the flow causes the sediments at the bed to be transported away. The amount of sediments that is transported is dependent of many factors i.a. the velocity of the flow and the sediment size, Centen (2015).

Sumer and Fredsøe (2005) describes seven phenomenons that can occur when a structure is placed in a marine environment:

1. the contraction of flow;
2. the formation of a horseshoe vortexes in front of the structure;
3. the formation of lee-wake vortices (with or without vortex shedding);
4. the generation of turbulence;
5. the occurrence of wave breaking;
6. the occurrence of reflection and diffraction waves; and
7. the pressure differentials in the soil that may produce "quick" conditions (liquefaction) allowing material to be carried off by currents.

These phenomenons can cause an increment in sediment transport, but transport of sediments does not mean that scouring will occur. Only when local sediment transport exceeds the supply of sediments from upstream, scour will develop. The difference in supply and erosion can occur due to the difference in velocity and/or turbulence.

2.3.2 Scour around a single slender pile

As described in earlier sections a structure placed in an marine environment it will change the flow around the structure. A single slender pile placed in an marine environment will be exposed to force from flow and waves which also interacts with the bed sediment. Research done by Sumer and Fredsøe (2005), Hoffmans and Varheij (1997) and others shows empirical relationships between the change in flow around an structure and the increase in bed shear stress close to the structure. The increase in shear stress is found to originate from a so called *Horseshoe Vortex* and *Lee-Wake Vortices* which develops around and behind the structure because of the change and rotation of the flow. Illustration of the horseshoe and Lee-wake vortexes is given in figure 2.3.

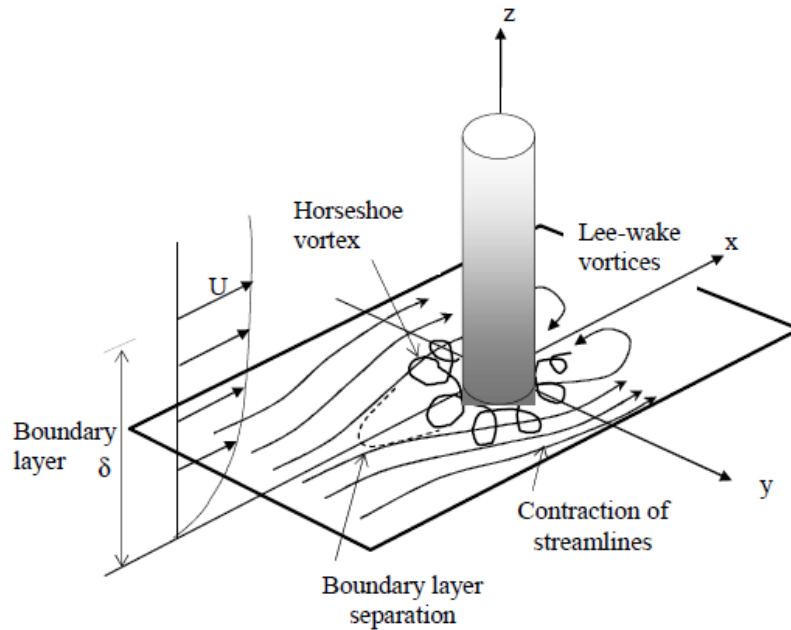


Figure 2.3: Development of horseshoe and Lee-wake vortices around a pile, from DNV (2014)

Horseshoe Vortex

The *Horseshoe Vortex* is caused by the rotation of the incoming flow due to the presence of the structure. The separated boundary layer "rolls-up" around the structure and form a spiral vortex around the structure hence the name "horseshoe vortex". Both laminar and turbulent horseshoe vortices exist and the horseshoe vortex is also present in waves. Sumer and Fredsøe (2005) states that the shear stress on the bed can be as high as 5 times the undisturbed bed shear stress, and as much as 11 times midway between the front and the side edges of the pile.

Lee-wake Vortices

The *Lee-wake vortices* is caused by the rotation of the boundary layer over the surface of the pile, where the shear layers of the flow roll up from the side of the pile in to the *lee wake* of the pile (i.e. the flow in the "back" side of the pile).

The scour in waves is governed by the horseshoe and lee-wake vortices. These are preliminary governed by the *Keulegan-Carpenter* number (KC) which is defined as:

$$KC = \frac{U_{max} \cdot T}{D} \quad (2.1)$$

Where:

U_{max} : maximum orbital velocity at the bed

T: wave period

D: diameter of pile

The maximum orbital velocity at the bed is given as:

$$U_{max} = \frac{\pi \cdot H}{T \sinh(kh)} \quad (2.2)$$

Where:

H: wave height

h: water depth

k: wave number

The wave number can be found by rearranging the following equation:

$$\left(\frac{2\pi}{T}\right)^2 = g \cdot k \tanh(kh) \quad (2.3)$$

Where:

g: the acceleration of gravity, $9,81 \text{ m/s}^2$

Clear water and live bed scour

Clear water scour is the name of the condition where there is no sediment movement far from the structure, e.i. there is only erosion (scour) close to the structure. Live bed scour is the name of the condition where there is sediment transport over the whole bed, e.i. erosion (scour) of the whole bed. This is described by Sumer and Fredsøe (2005) as the ratio between the undisturbed Shields parameter (θ) and the critical Shields parameter (θ_{cr}). The critical shields parameter is the shields parameter where the bed starts to erode ($\tau_o = \tau_{cr}$). The critical shear stress (τ_{cr}) can be found with a *Shields diagram*.

Clear water scour:

$$\theta < \theta_{cr} \quad (2.4)$$

Live bed scour

$$\theta > \theta_{cr} \quad (2.5)$$

The Shields parameter θ is described as:

$$\theta = \frac{U_f^2}{g(s-1)d} \quad (2.6)$$

By DNV (2014) the bed shear velocity, U_f , is defined by:

$$\frac{U_c}{U_f} = 6,4 - 2,5 \cdot \ln\left(\frac{2,5 \cdot d}{h} + \frac{4,7 \cdot \nu}{h \cdot U_f}\right) \quad (2.7)$$

Where:

d: grain size

h: height

ν : kinematic viscosity ($10^{-6} \text{ m}^2/\text{s}$)

U_f : steady current base velocity

U_c : current velocity

For waves the base velocity is given as:

$$U_f = \sqrt{\frac{f_w}{2}} \cdot u_{max} \quad (2.8)$$

Where f_w is the frictional coefficient given by:

$$f_w = \begin{cases} 0,04 \cdot (a/k_N)^{-0,25} & \text{for } a/k_N > 100 \\ 0,4 \cdot (a/k_n)^{-0,75} & \text{for } a/k_N < 100 \end{cases} \quad (2.9)$$

and

$$a = \frac{u_{max} \cdot T}{2\pi} \quad (2.10)$$

Here k_N is the bed roughness which is equal to $2,5 \cdot D_{50}$ and d_{50} is the median grain size in the particle size distribution of the bed material. DNV (2014) states that the equilibrium scour depth can be used for structural design, but may be supplemented with an extra safety margin.

2.3.3 Calculation of scour depth

The scour depth is dependent on the material around the pile, the shape of the pile and whether it is exposed to current only, waves or both current and waves. DNV (2014) gives guidelines for the calculation of scour depth and the following procedure is recommended in situations where no model data is available.

The equilibrium scour depth can be expressed by:

$$S/D = 1,3\{1 - \exp[-0,03(KC - 6)]\} \quad KC \geq 6 \quad (2.11)$$

Where:

KC: Keulegan-Carpenter number

S: scour depth

D: diameter of pile

This expression is valid for live bed scour i.e $\theta > \theta_{cr}$. For steady currents where $KC \rightarrow \infty$, the ratio $S/D \rightarrow 1,3$. From equation 2.3.3 there will not be any scour when $KC < 6$ due to no formation of horseshoe vortex.

Extension of the scour hole

The scour hole extension can be calculated when considering the *friction angle* of the material assuming that the slope of the scour hole is at the angle of repose:

$$r = \frac{D}{2} + \frac{S}{\tan\phi} \quad (2.12)$$

Where:

r: radius of the scour hole from the centre of the pile diameter

D: diameter of the pile

S: scour depth

ϕ : friction angle of the material

2.4 Theoretical Background for Foundation Design

This chapter explains the background theory of the foundation design and includes the formulation of the p-y curves used in the current design approach. Foundations for offshore wind turbines has been subject to a lot of research in recent years. Work done by Kallehave (2015); Hanssen (2016) intend to improve the formulation for calculating the response of the foundation. The approach described in the standard for designing foundations for offshore wind turbines relies on p-y curves for determining the lateral response of the monopile foundation, but the current formulation of p-y curves is based on slimmer and slender piles than those used in the offshore wind industry, and Kallehave (2015) has measured that when using the formulation in DNV (2014) there is up to 20 % difference when comparing the calculated eigenfrequency of a wind turbine with the measured value.

2.4.1 Formulation of p-y curves

The current design approach is based on p-y curves representing the lateral response of the soil surrounding the pile when exposed to a lateral load. The method is described in DNV (2014); API (2011) and is widely adopted in the offshore wind industry. The p-y analysis is an numerical model that simulates the soil as non-linear springs where p is the soil pressure per unit length of pile and y is the pile deflection. From this model the soil can be illustrated with a series of non-linear *p-y curves* that can vary with depth and soil type (DFI, 2013).

The model was first developed in the 1940's and 50's when oil companies needed to build offshore structures that could withstand heavy horizontal loads from wind and waves. Matlock (1970) conducted a series of experiments on piles in soft clay and came up with an empirical relationship between the soil pressure and lateral displacement.

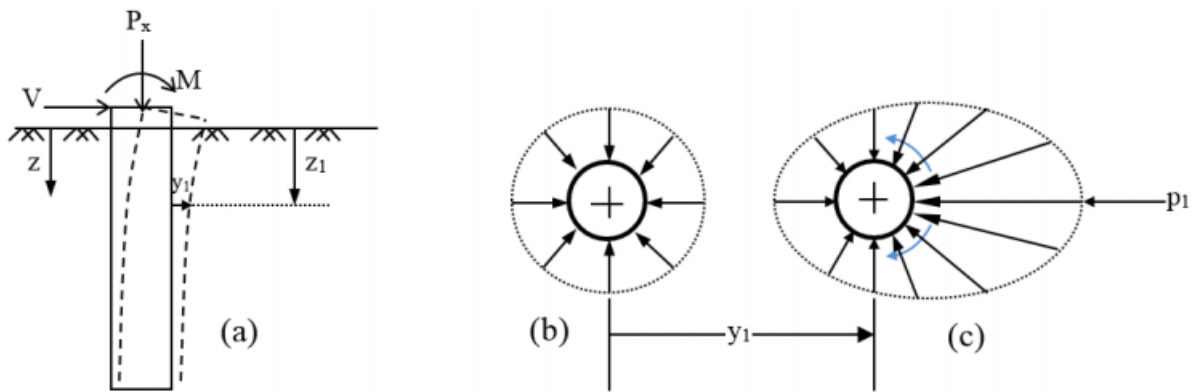


Figure 2.4: Stress distribution in a laterally loaded pile. from Rocscience (2016).

Figure 2.4 shows a pile under lateral loading. When unloaded there is a uniform stress distribution normal to the pile as shown in figure 2.4b. When the pile is subject to a lateral load the pile deflects a distance y_1 at a depth z_1 and the stress on the backside of the pile has decreased and the stress on the front of the pile has increased, inducing the resistance force p_1 which consists of both normal and shearing components as the soil tries to move around the pile. The new stress situation is shown in figure 2.4c (Rocscience, 2016).

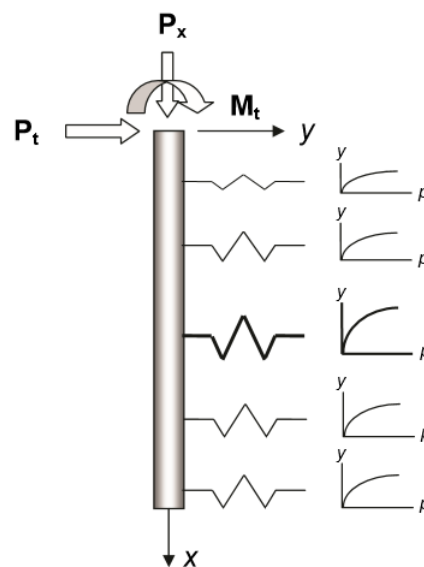


Figure 2.5: Concept of soil response curves for a laterally loaded pile, from FHWA (2010).

The formulation of p - y curves has been divided into two formulations for respectively soft clay and sand with different formulations for static and dynamic loading in clay.

Lateral capacity in soft clay

The principle of p - y curves has been adopted by the *American Petroleum Institute (API)* and *DNV GL* which have included this in their standards for offshore structures.

The unit lateral capacity, p_r , of soft clay, in units of force per unit length is found to vary between $8 \cdot c_u \cdot D$ and $12 \cdot c_u \cdot D$ except for shallow depth where the failure mechanism is different

due to low stress from the overburden (ISO, 2007).

p_r increases from $3 \cdot c_u \cdot D$ to $9 \cdot c_u \cdot D$ as X increases from 0 to X_R according to equation 2.13:

$$p_r = 3 \cdot c_u \cdot D = p'_0 \cdot D + J \cdot c_u \cdot X \quad (2.13)$$

p_r is limited by equation 2.14:

$$p_r = 9 \cdot c_u \cdot D \quad \text{for } X > X_R \quad (2.14)$$

where:

p_r : is the representative lateral capacity in units of force per unit length;

c_u : is the undrained shear strength in stress units;

D : is the diameter of the pile;

p'_0 : is the effective overburden stress at depth X ;

J : is a dimensionless parameter with values ranging from 0,25 to 0,5 having been determined by field testing. If no other information is available common practise is to use 0,5;

X : is the depth below the sea floor;

γ' : is the submerged unit weight of the soil;

X_R : is the depth below the sea floor to the bottom of a reduced resistance zone given by equation 2.15;

$$X_R = \frac{6 \cdot c_u \cdot D}{\gamma' \cdot D + J \cdot c_u} \quad (2.15)$$

In the case of non-uniform soils equation 2.13 and 2.14 can be solved by plotting the two equations for p_r against *depth*. The first point where the two equations intersect is then X_R . In general X_R is 2,5 times the pile diameter (ISO, 2007).

p-y curves for soft clay

The relationship between soil resistance and displacement for piles in soft clay is generally non-linear. P-y curves is by ISO (2007) generated from a given set of values for p/p_r and y/y_c , these values changes for static and dynamic loading.

Short term static loading

where:

p_r : lateral capacity in units force per unit length

p : mobilised lateral resistance in unit force per unit length

y : local lateral displacement

y_c : $2,5 \cdot \epsilon_C \cdot D$

Table 2.2: Mobilised lateral resistance - displacement for short-term static loading, from ISO (2007)

p/p_r	y/y_c
0,00	0,0
0,23	0,1
0,33	0,3
0,50	1,0
0,72	3,0
1,00	8,0
1,00	∞

D : pile diameter

ϵ_C : strain at 0,5 of maximum deviatoric stress in uniaxial compression test

In the case where equilibrium has been reached under cyclic actions p-y curves can be generated from table 2.3.

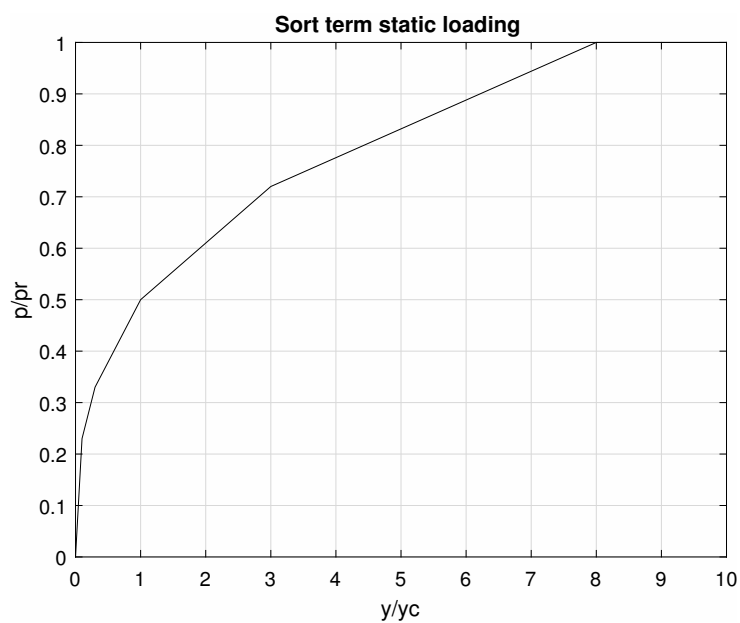


Figure 2.6: Short term static loading, after ISO (2007).

Short term dynamic loading

Table 2.3: Mobilised lateral resistance - displacement for short-term cyclic loading, from ISO (2007)

$X > X_R$		$X < X_R$	
p/p_r	y/y_C	p/p_r	y/y_C
0	0	0	0
0,23	0,1	0,23	0,1
0,33	0,3	0,33	0,3
0,50	1,0	0,50	1,0
0,72	3,0	0,72	3,0
0,72	∞	$0,72X/X_R$	15,0
		$0,72 X/X_R$	∞

where:

X : depth below sea floor

X_R : depth below the sea floor to bottom of reduced resistance zone (see equation 2.15)

p_r : lateral capacity in units force per unit length

p : mobilised lateral resistance in unit force per unit length

y : local lateral displacement

y_C : $2,5 \cdot \epsilon_C \cdot D$

D : pile diameter

ϵ_C : strain at 0,5 of maximum deviatoric stress in uniaxial compression test

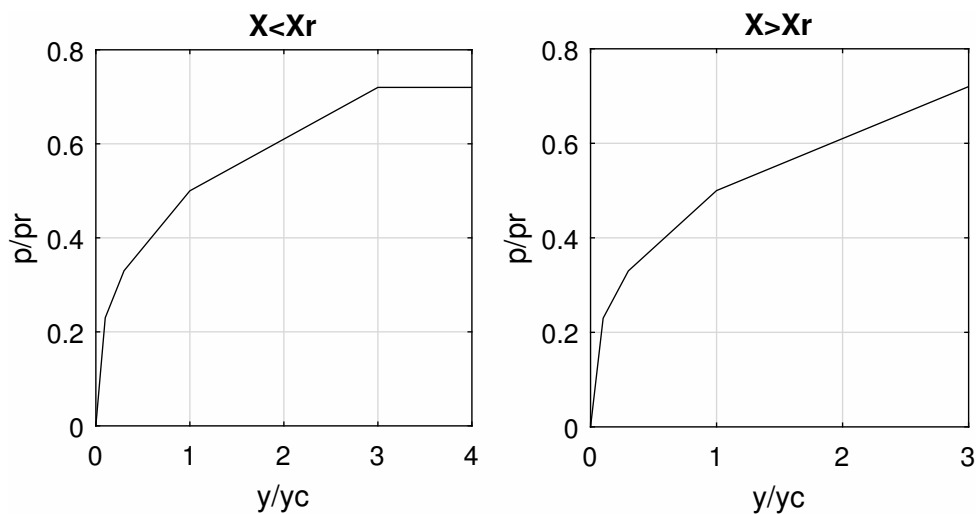


Figure 2.7: Short term dynamic loading, after ISO (2007).

These equations and tables can be used to construct a p - y curve for a given condition.

Lateral capacity in sand

By following the API standard the lateral soil resistance, p , as a function of the lateral deflection, y , is assumed to be (Kallehave, 2015):

$$p(y) = Ap_u \tanh\left(\frac{kz}{Ap_u} y\right) \quad (2.16)$$

Where:

k : initial modulus for sub-grade reaction

z : depth

p_u : modified ultimate soil resistance

The empirical strength parameter A is given by the following statement:

$$A = \begin{cases} 0,9 & \text{cyclic} \\ (3 - 0,8 \frac{x}{D}) \geq 0,9 & \text{static} \end{cases} \quad (2.17)$$

The modified ultimate resistance, p_u is:

$$p_u = \min \begin{cases} (c_1 z + c_2 D) \gamma z \\ c_3 D \gamma' z \end{cases} \quad (2.18)$$

Where:

c_1, c_2, c_3 : factors depending on internal friction of the sand (see figure 2.8a)

D : diameter of the pile

γ' : effective soil weight

c_1, c_2, c_3 can also be found with the following equations:

$$c_1 = \frac{(\tan \beta)^2 \tan \alpha}{\tan(\beta - \phi')} + K_0 \cdot \left[\frac{\tan \phi' \cdot \sin \beta}{\cos \alpha \cdot \tan(\beta - \phi')} + \tan \beta \cdot (\tan \phi' \cdot \sin \beta - \tan \alpha) \right] \quad (2.19)$$

$$c_2 = \frac{\tan \beta}{\tan(\beta - \phi')} - K_a \quad (2.20)$$

$$c_3 = K_a \cdot [(\tan \beta)^8 - 1] + K_0 \cdot \tan \phi' \cdot (\tan \beta)^4 \quad (2.21)$$

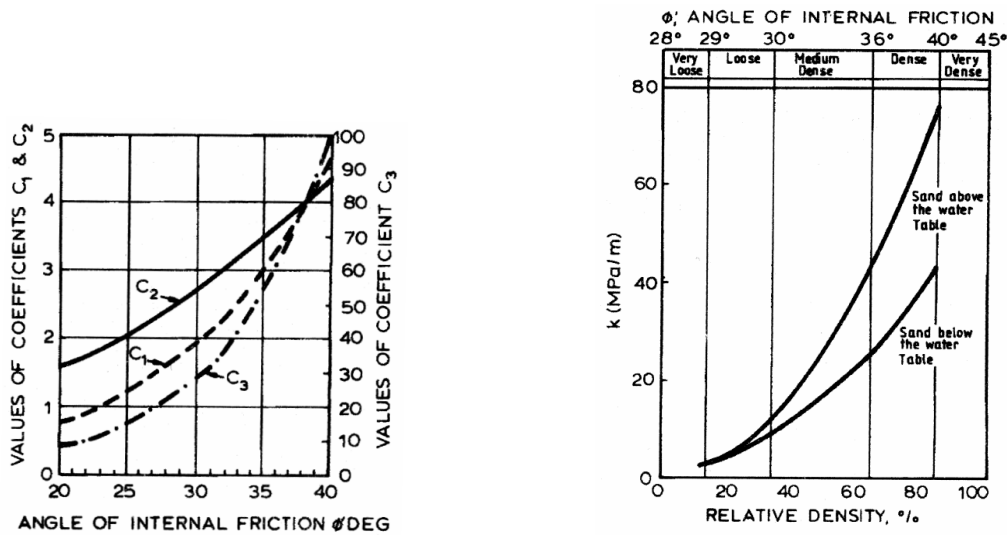
where:

$$\alpha = \frac{\phi'}{2}$$

$$\beta = 45 + \frac{\phi'}{2}$$

$$K_0 = 0,4$$

$$K_a = \frac{1 - \sin \phi'}{1 + \sin \phi'}$$



(a) Coefficients as function of friction angles. (b) Initial modulus of subgrade reaction k as function of friction angle ϕ .

Figure 2.8: Graphs to determine the c and k coefficients, from API (2011).

The k from equation 2.16 can be found by plotting the table with the rate of increase on the initial subgrade reaction with depth from API (2011) and calculating an equation for the graph.

ϕ' [°]	k [MN/m^3]
25	5,4
30	11
35	22
40	45

Table 2.4: Rate of increase with depth of initial modulus of subgrade reaction, from API (2011).

The data in table 2.4 can be fitted by the eq. 2.22:

$$k = 0,1589e^{0,0832\phi} \tag{2.22}$$

From the p - y curves it is possible to find the stiffness of the soil layer by looking at the initial slope of the p - y curve:

$$E_0^{py} = p'(0) = kz \tag{2.23}$$

2.4.2 Modification of p-y curve formulation

Kallehave (2015) states that the current procedure for calculating p-y curves based on API and DNV GL standards underestimates the stiffness of the soil. After evaluation a series of instrumented offshore wind turbines Kallehave (2015) found that the natural frequency of the structures was 5-7 % higher than predicted using the standard methods. The difference in design and observed natural frequency concludes that the methods used in current design codes is a crude approximation and is not very accurate for large diameter, short piles used in the offshore wind industry.

To assess the possibility of modifying the current formulation, Kallehave (2015) investigated the governing parameters of the shape of the p-y curve, effects from strain level and stiffness profile. The findings was used to modify the formulation to take into account the difference in size and depth when comparing the basis for the p-y formulation from Matlock (1970); DNV (2014) with the size and depth of monopiles used in the offshore wind industry.

Since σ'_v is proportional to Z Kallehave (2015) suggested that the depth effect could be formulated as:

$$E_0^{py} \propto z_0 \left(\frac{z}{z_0} \right)^n \quad (2.24)$$

Where:

z_0 : the reference depth from the original formulation (2,5 m)

n : a site specific parameter expected to be in the range of 0,4-0,7

For the strain level effect Kallehave (2015) suggest to use a formulation by Stevens and Audibert (1979):

$$E^{py} \propto E_0^{py} \left(\frac{D}{D_0} \right)^{m(y)} \quad (2.25)$$

Where:

- D_0 : reference diameter (0,61m)
- E_0^{py} : initial soil stiffness
- m : diameter exponent

Stevens and Audibert (1979) suggest using $m = 0,5$ for clay. For larger diameter monopiles Kallehave (2015) gives some realistic values for y (see table 2.5). The nonlinear formulation of the stiffness degradation leads to the change in m , this is why the highest value of m are applied in the top layers of the soil and the smaller values are applied in the lower layers of the soil.

Table 2.5: Diameter exponent for varying displacement, from Kallehave (2015).

y [mm]	1,0	2,5	5,0	7,5	10,0
m	0,29	0,41	0,52	0,58	0,63

Kallehave (2015) states that the use of $m = 0,5$ give an underestimating of the stiffness of the top soil layers and overestimating the stiffness of the lower layers.

Modified formulation

To take in to account the physical differences between the test done by Matlock (1970), Kallehave (2015) modifies the original formulation in equation 2.4.1 to include the effects of strain and depth formulated in equation 2.4.2 and 2.4.2:

$$E_{mod}^{py} = kz_0 \left(\frac{z}{z_0} \right)^n \left(\frac{D}{D_0} \right)^{0,5} \quad (2.26)$$

To evaluate the new formulation Kallehave (2015) conducted a benchmark study against full-scale measurements from the offshore wind turbines mentioned earlier. The result was an deviation in the natural frequency of 2-4% compared to the observed values. This shows an improvement over the 5-7% deviation from the original API formulation.

2.5 Effect of Cyclic Loading on Lateral Response

This chapter present recent research on the effect of cyclic loading on the lateral response of monopile foundations for offshore wind turbines. Monopiles placed in an marine environment is exposed to many different cyclic loads from both rotor and environmental loads. To adequately assess the performance of the structure it is important to take in to account the effect of cyclic loading on the fatigue of the structure and surrounding soil. Under-prediction of the effect of cyclic loading on the degradation of the surrounding soil can effectively increase the fatigue on the structure and in worst case lead to total breakdown of the structure.

Cyclic loads on offshore wind turbines

As stated in section 2.1.1 an offshore wind turbine is exposed to cyclic loads, 1P and 3P, which is used to tune the eigenfrequency of the structure to fit in between these frequency ranges. Achmus et al. (2009) states that the numbers of cyclic loads due to wind and waves could exceed 10^8 over the lifetime of the structure. Cyclic loads leads to accumulation of pile head displacements and rotations which can come in conflict with SLS described in section 2.1. The standard method for calculation the pile head displacements is by using p-y curves, but according to Achmus et al. (2009) these are based on field test with less than 200 cycles.

Cyclic degradation of soil stiffness

Recent research done by Achmus et al. (2009); Kim et al. (2015) shows a clear degradation of soil stiffness over time based on different cyclic loads and amplitudes. Achmus et al. (2009) states that the accumulation of plastic strain in cyclic triaxial test can be interpreted as a decrease in soil secant stiffness. Different methods has been applied to evaluate the effect of cyclic loading on the lateral displacement. Achmus et al. (2009) developed design charts for offshore wind turbines placed in sandy soils based on a stiffness degradation model. Kim et al. (2015) used some of the results from Achmus et al. (2009) in their research to evaluate the effect of cyclic loading, but by using a *strain wedge model* (SWM). The model is based on a kinematic model with the formation of a 3-D wedge formed on the passive side of the pile and is used to calculate the soil resistance against lateral loading. The wedge configuration is determined by the mobilised friction angle and pile diameter.

The SW model is by Kim et al. (2015) configured according to figure 2.9 where:

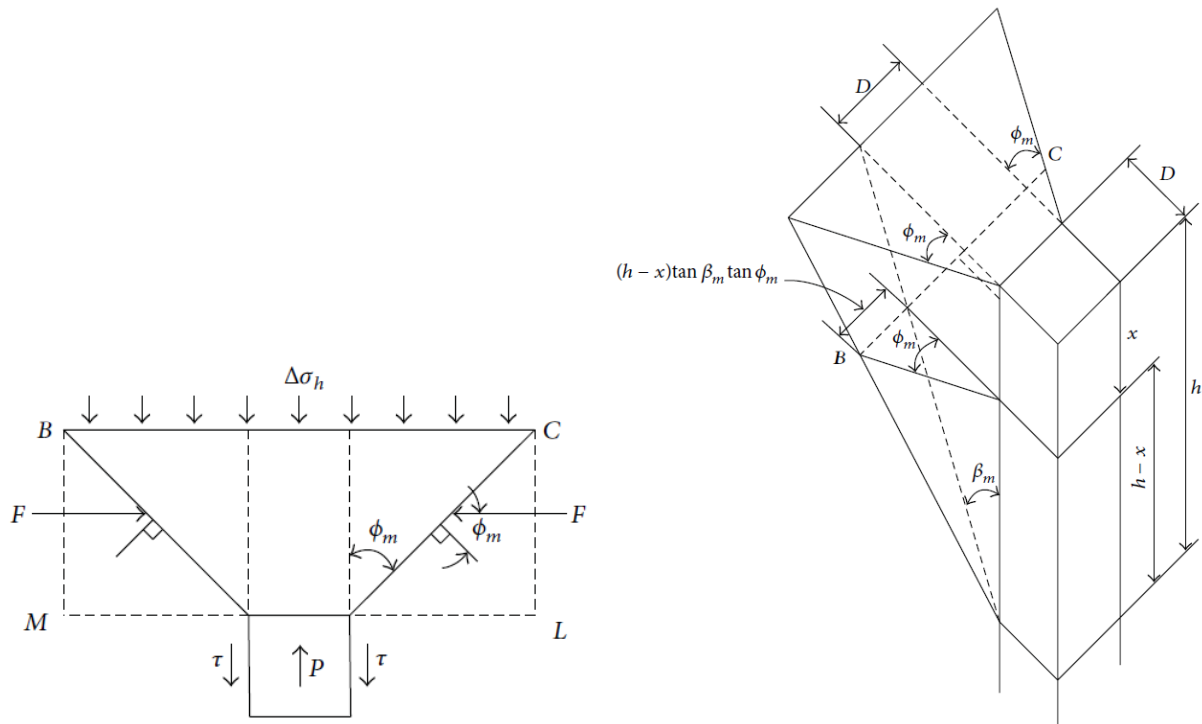


Figure 2.9: Strain wedge in uniform soil, from Kim et al. (2015).

$$\beta_m = 45^\circ + \phi_m/2$$

ϕ_m : mobilised friction angle of the soil

D: diameter of the pile

h: height of the passive wedge

$\Delta\sigma_h$: variation in horizontal force in the wedge face

τ : shear stress at pile side

x: depth below top of passive wedge

P: lateral load

The model is used to evaluate the lateral response of a pile in a given uniform soil layer. The soil that was chosen had a peak internal friction angle of $37,5^\circ$ and a unit weight of $11 \text{ kN}/\text{m}^3$ and cohesion of 0 kPa. The cyclic load was chosen to be 25%, 50 % and 75 % of Q_u , where Q_u was found to be 22.04 MN at 38,1 mm of lateral displacement. After a certain number of cycles the pile was loaded laterally with Q_u to obtain the relationship between the load and displacement, (Kim et al., 2015).

Results from the SWM analysis is presented in figure 2.10 and show a clear degradation of soil stiffness with number of cycles and load intensity. The pile was more displaced as the number of cycles increased. The results of Kim et al. (2015) shows up to 40 % more deflection with higher number of cycles and lateral load. Compared to the design criteria the partial factor for lateral resistance $\gamma_m = 1,0$ according to DNV (2014) in section 2.2.

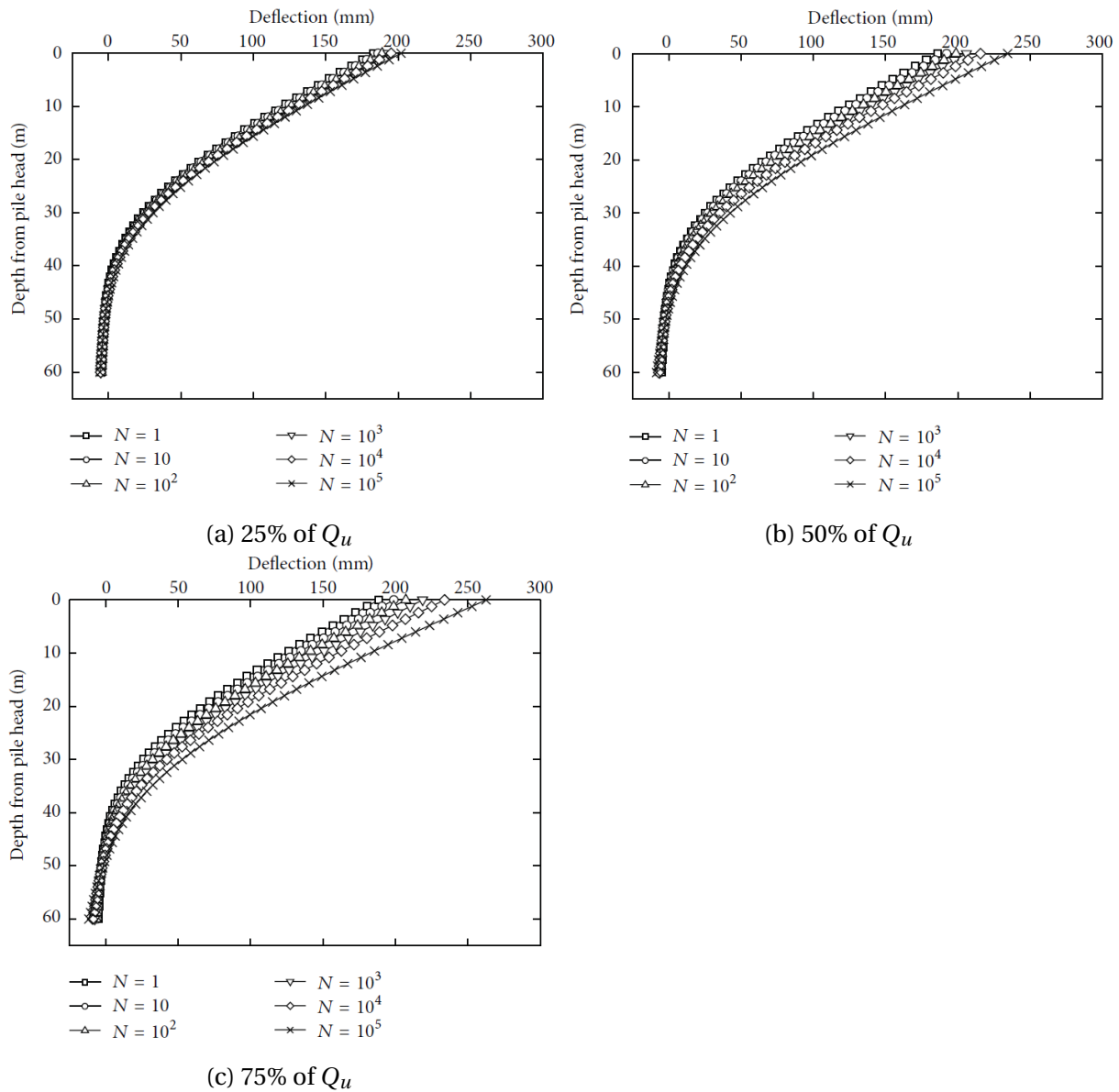


Figure 2.10: Pile deflection curves for 3 cyclic lateral loads: (a) 25%, (b) 50%, and (c) 75% of the static capacity (Q_u), from Kim et al. (2015).

Parametric study

In relation to the work with the degradation stiffness model and design charts for cyclic loading Achmus et al. (2009) conducted a parametric study to quantify the effect of geometry, subsoil and loads on the response of the monopile.

The following ranges of parameters was considered, from Achmus et al. (2009):

- Pile geometry: embedded length L : 20-40 m, diameter D : 2,5-7,5 m, pile wall thickness $t_p = 0,09$ m.
- Loading: lateral load H : 5-30 MN, moment arm h : 0-40 m, number of cycles N : 1-10.000.
- Soil types: dense sand and medium dense sand.

The results from the parametric study was used to develop design charts for both static and dynamic loading were developed. Achmus et al. (2009) concludes that the lateral deflection is very much dependent on the load level, the ratio between the load and ultimate load capacity. Since the ultimate load is very much dependent on the embedded length, the accumulated deflection for a given load is dependent on the embedded length of the pile. The pile diameter also effects the ultimate load capacity, but not as much as the embedded length.

Model Used in Simulations

This chapter describes the model used to simulate a monopile placed in sand with scour protection. The simulations was done in Plaxis 3D with the *Hardening Soil Small* (HSS) soil model which is included in the software. The HSS model is specialised in capturing the small strain stiffness of the soil, which is the governing factor in the lateral response of the soil around offshore wind turbines. The soil properties used in the simulations is similar to *Hokksund* sand. This particular sand has been used as models and for the Norwegian University of Science and Technology (NTNU) for over 30 years (Hanssen, 2016).

3.1 Hardening Soil Small Soil Model

The Hardening soil small (HSS) model is a default soil model in Plaxis 3D and is used to investigate the stiffness in the small strain area. The main features of the model is, after Hanssen (2016):

- Stress dependent stiffness according to a power law
- Plastic strains due to deviatoric loading
- Plastic strains due to primary compression
- Mohr-Columb failure criterion
- Small-strain stiffness and a nonlinear dependency on strain amplitude and strain history
- Threshold strain between small-strains and larger strains

The HSS soil model is developed by Benz (2007) and is a continuation of the HS soil model with improved formulations in the small strain area.

3.2 Soil properties

The Hokksund sand is a uniform, medium grained quartz sand from a natural deposit in Hokksund (Norway). The properties of the sand is described in table 3.1.

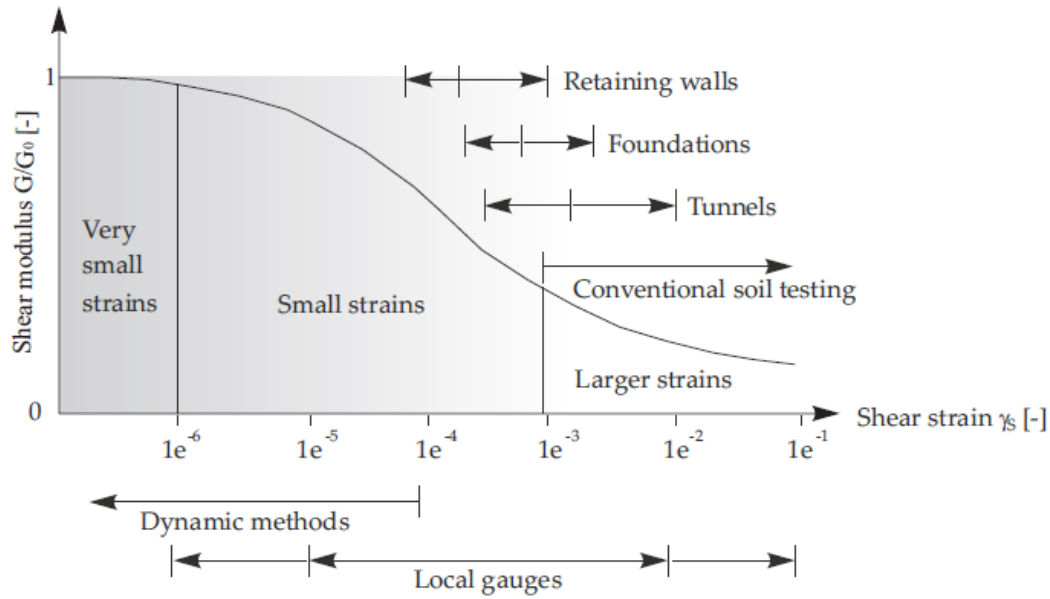


Figure 3.1: Characteristic stiffness-strain behaviour of soil with typical strain ranges for structures and laboratory tests, from Plaxis (2016).

Parameter	Unit	Value
Internal friction angle	[°]	38
Porosity (n)	[%]	39,9
Min. porosity (n_{min})	[%]	36,4
Max. porosity (n_{max})	[%]	48,8
Relative density (D_r)	[%]	76
Density (γ)	[kN/m^3]	16,0
Specific density (γ_s)	[kN/m^3]	27,1
Coefficient of uniformity (C_u)	[-]	2,04
Mean grain size (d_{50})	[mm]	0,38

Table 3.1: Key soil parameters of Hokksund sand, after Hanssen (2016).

3.2.1 Linear Elastic Soil with Stiffness from Oedometer Testing

Both Moen (1978); Sandven (1992) have tested the Hokksund sand in oedometer to obtain the soil stiffness. The stiffness can be described with Janbu's equation for stress dependent stiffness:

$$M_s = m \cdot \sigma_a \left(\frac{\sigma'}{\sigma_a} \right)^{1-\alpha} \tag{3.1}$$

Where:

M_s : constraints modulus of the soil

m : modulus number

σ_a : reference stress, 100 kPa

σ' : effective vertical stress

α : stress exponent

From the results obtained by Moen (1978); Sandven (1992) the modulus number $m = 500$ and $\alpha = 0,5$ has been given for the sand. The Young's modulus, E_s , is calculated using elasticity theory where Possion's ratio ν is assumed to be 0,2. Figure 3.2 shows the development of the Young's modulus with depth.

$$E_s = M_s \cdot \frac{(1 + \nu)(1 - 2\nu)}{(1 - \nu)} \quad (3.2)$$

Where:

E_s : Young's modulus

ν : Possion's ratio

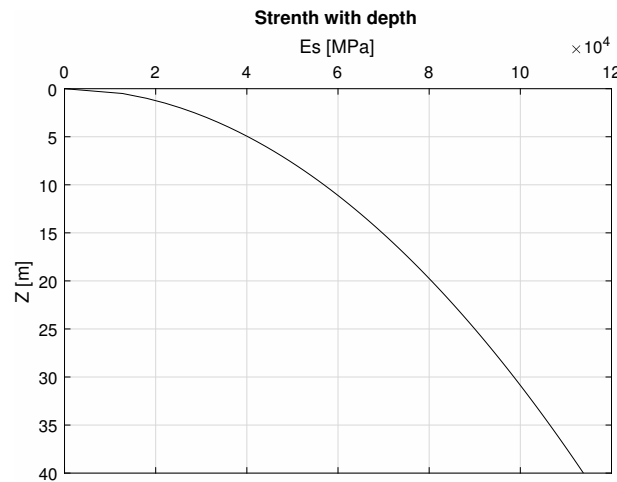


Figure 3.2: Change in E_s with depth according to eq. 3.2.

3.2.2 HSS with Stiffness from SWV and Oedometer

The soil parameters used in the HSS model is based on shear-wave velocity measurements and the oedometer stiffness described in eq. 3.1. The stress dependent stiffness in the HSS model is given by eq. 3.3, 3.4 and 3.5.

$$E_s = E_{s,50}^{ref} \left(\frac{c \cos \varphi - \sigma'_3 \sin \varphi}{c \cos \varphi + p_{ref} \sin \varphi} \right)^m \quad (3.3)$$

$$G_{s,max} = G_{s,max}^{ref} \left(\frac{c \cos \varphi - \sigma'_3 \sin \varphi}{c \cos \varphi + p_{ref} \sin \varphi} \right)^m \quad (3.4)$$

$$M_s = M_{s,50}^{ref} \left(\frac{c \cos \varphi - \frac{\sigma'_3}{K_o^{nc}} \sin \varphi}{c \cos \varphi + p_{ref} \sin \varphi} \right)^m \quad (3.5)$$

Share wave velocity measurements

To find the small strain shear modulus G_{max} Hanssen (2016) used *shear-wave velocity* measurements with different vertical stresses from 8-58 kPa. The formula used to calculate the small strain shear modulus from the shear wave velocities is given in eq. 3.6.

$$G = v_s^2 \rho \quad (3.6)$$

Where:

v_s : shear wave velocity [m/s]

ρ : density [kg/m^3]

From the SWV results Hanssen (2016) fitted an equation to the points obtained from eq. 3.6 to get an expression for the small strain modulus dependent on the vertical stress. The expression is given in eq. 3.7.

$$G_s = g(p_{ref}\sigma'_v)^{0,5} + k \quad (3.7)$$

Where:

G_s : small strain modulus

g : 1000

p_{ref} : 100

k : 39000

The results from the measurements of shear-wave velocity measurements and the calculated G_{max} fitted with eq.3.7 for a σ_v up to 60 kPa is given in figure 3.3.

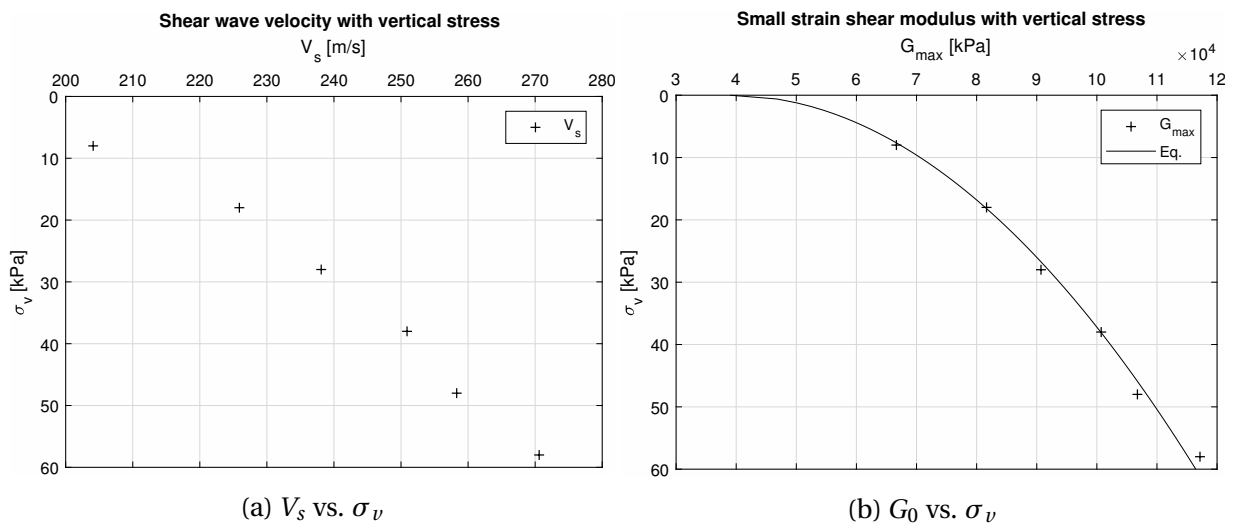
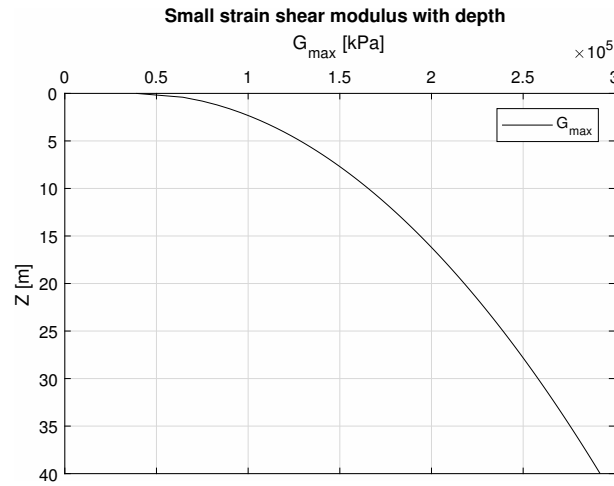


Figure 3.3: (a) Measured shear wave velocity against vertical stress and (b) calculated small strain modulus against vertical stress, after Hanssen (2016).

The results from the measurements with the corresponding equation is used to calculate the small strain modulus down to 40 m and the parameters is assumed to be the same as for Hanssen (2016). In Plaxis the following parameters should be included, $E_{s,50}^{ref}$, $M_{s,50}^{ref}$, $E_{s,ur}^{ref}$, $G_{s,50}^{ref}$ and $\gamma_{0,7}$ as given in eq. 3.3 - 3.5. The results for G_{max} from the SWV measurements is used as reference for calculating the parameters, see appendix A.

The HSS model also incorporates a threshold shear-strain $\gamma_{0,7}$ which is given by eq. 3.8:

Figure 3.4: Small strain modulus G_{max} with depth

$$\gamma_{0,7} = \frac{1}{9G_{s,max}} \left[2c(1 + \cos(2\varphi)) + \sigma'_1(1 + K_0)\sin(2\varphi) \right] \quad (3.8)$$

Where:

$G_{s,max}$: shear modulus at small strains

c : cohesion

φ : friction angle

σ'_1 : effective vertical stress

K_0 : earth pressure coefficient at rest

A summary of the input parameters for the HSS model is described in table 3.2.

Table 3.2: Parameters for the HSS model, after Hanssen (2016)

Symbol	Unit	Value
ϕ	[°]	38
c'_{ref}	[kPa]	1,0
$E_{s,50}^{ref}$	[MPa]	64,2
$M_{s,50}^{ref}$	[MPa]	50
$E_{s,ur}^{ref}$	[MPa]	190
γ'	[kN/m ³]	6
m	[-]	0,38
$\nu'_{s,ur}$	[-]	0,2
ψ	[°]	0

3.3 3D-FEM model in Plaxis

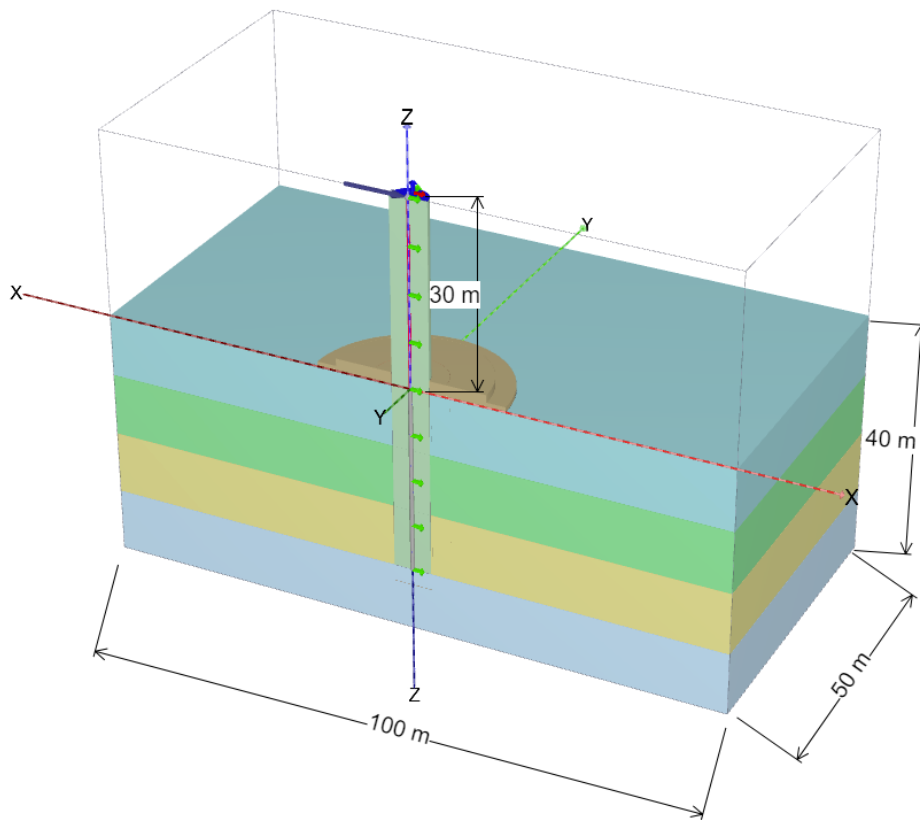


Figure 3.5: Model from Plaxis with scour protection layer.

The model used in the simulations is a 3D-FEM model of a pile placed in sand. The size of the model is chosen to be close to real situation with a 60 m long pile with diameter of 6 m, embedded 30 m in sand. To reduce the calculation time only half of the geometry is modelled, using symmetry boundary conditions along the symmetry line (x-z plane). The soil has also been divided into 4 layers of 10 m height to be able to vary the threshold shear strain ($\gamma_{0,7}$) with depth. In the model it's used medium coarse mesh with mesh refinement close to the pile and within the pile to prevent numerical errors. Figure 3.5 shows the model used in the simulations.

3.3.1 Pile Geometry

The pile used in the simulations is selected to represent a real situation with characteristic size and properties from Kallehave (2015); Hanssen (2016). The pile is modelled with volume elements with an equivalent Young's modulus which is given by:

$$E^* = E \left(1 - \left(\frac{r-t}{r} \right)^4 \right) \quad (3.9)$$

Where:

r: radius of the pile

- t: thickness of the pile walls
- E: Young's modulus of the pile material
- E^* : Equivalent Young's modulus

Table 3.3: Pile properties

	Unit	Value
Pile diameter (D)	[m]	6
Embedded length (L)	[m]	30
Total length	[m]	60
Wall thickness (t)	[mm]	80
Unit weight	[kg/m^3]	7850
Young's modulus (E_{steel})	[GPa]	210
Equivalent Young's modulus E^*	[GPa]	21,5
Possion's ratio (ν)	[-]	0,3
Interface roughness (α)	[-]	1

The pile is modelled by 10-noded triangular volume elements. The pile elements is modelled with a linear-elastic material law with equivalent bending stiffness and unit weight as a as a pile with open centre (pipe-like structure). 10-noded triangular elements of zero thickness is placed between the pile and the soil as a interface with interface roughness $\alpha = 1$. An illustration of the model is shown in figure 3.5. To extract the bending moment from the model a soft beam is placed in the centre of the pile. The beam has no weight or stiffness and will not contribute to the overall stiffness of the pile. The idea is that the beam will mimic the soil behaviour along the pile. In Plaxis the moment distribution along the beam and deflection of the beam can easily be extracted for further calculations.

3.3.2 Properties of Scour Protection Layer

The properties of the scour protection layer is selected to represent a real situation with characteristic size and properties and is based on conditions described by Kallehave (2015). The scour protection layer is modelled with HSS soil model with similar properties as the upper layer of Hokksund sand. The scour protection layer generally consists of stones placed around the pile, and the layer is characterised with high stiffness. To accommodate this the cohesion, C , is increased to 20 kPa to simulate the higher strength of the material compared to the layer beneath.

Since the cohesion is increased the development of $G_{0,HSS}$ and γ_{07} with depth also changes. The change is presented in figure 3.6.

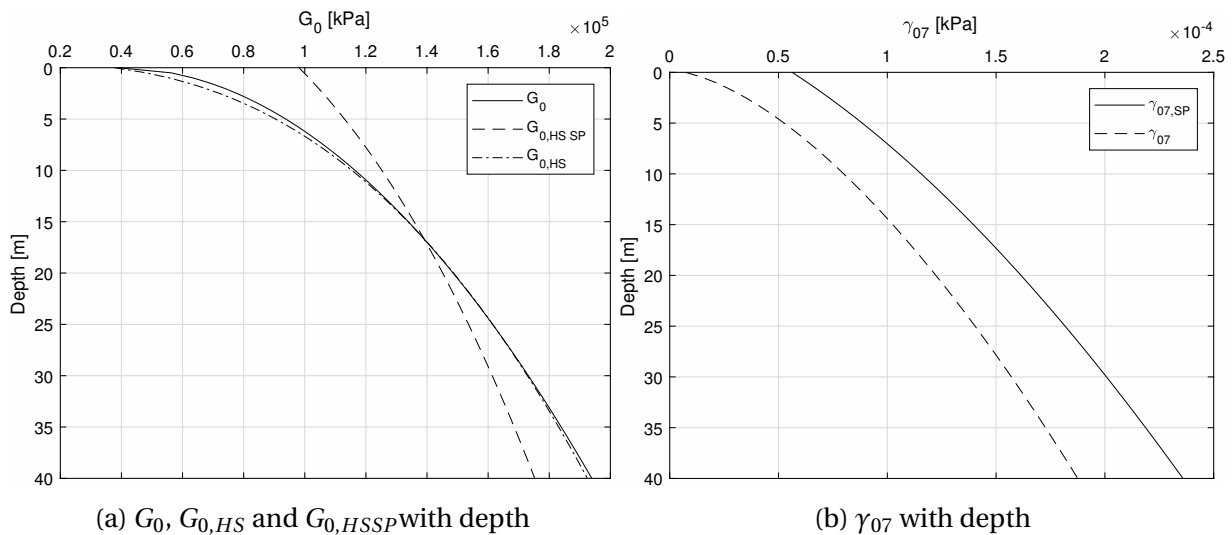
The HSS parameters for the scour protection layer is chosen to be the same as for the first layer of Hokksund sand but with increased cohesion. The HSS parameters for the first layer of Hokksund sand is taken from a depth of 5 m.

3.3.3 Load characteristics

In operation, the load on the pile is generated from the weight of the tower structure, cyclic loads from wind and waves acting on the pile and tower structure and cyclic loads from the rotor (1P and 3P). To assess the soil response the pile is exposed to a range of loads, 10 kN,

Table 3.4: Parameters for the HSS model of the scour protection layer.

Symbol	Unit	Value
ϕ	[°]	38
c'_{ref}	[kPa]	20,0
$E_{s,50}^{ref}$	[MPa]	64,2
$M_{s,50}^{ref}$	[MPa]	50
$E_{s,ur}^{ref}$	[MPa]	190
γ'	[kN/m ³]	6
m	[-]	0,38
$\nu'_{s,ur}$	[-]	0,2
ψ	[°]	0
Radius of filter layer (R_F)	[m]	2,5D
Radius of armour layer (R_A)	[m]	2,0D
Thickness of filter layer (h_F)	[m]	0,8
Thickness of armour layer (h_A)	[m]	1,2

Figure 3.6: Change in G_0 , $G_{0,HS}$, $G_{0,HSSP}$ and γ_{07} with depth down to 40 m for the scour protection layer.

100 kN, 1000 kN, 2000 kN and 5000 kN. The load steps is chosen to represent a variation of load cases from very small loads to bigger loads. The last load step, 5000 kN, is selected because of computational reasons as bigger load will increase the calculation time and the loads selected gives satisfactory results and is sufficient to construct p-y curves. The load steps is applied as static loads at the top of the pile.

3.4 Simulation Staging in Plaxis

The simulation in Plaxis is divided in to three different cases to analyse the effect scour protection on the lateral behaviour of the pile. First the simulations is done without any scour protection, second the scour protection is modelled as surface load and finally the scour protection is modelled as a layer on top of the subsoil.

3.4.1 Benchmark Study Without Scour Protection

In the first case the monopile and soil is modelled without any form of scour protection around the pile. This is to simulate a benchmark condition which later will be used to analyse the effect of the scour protection on the lateral response of the soil. The case is divided into 5 load steps as described in section 3.3.3.

3.4.2 Scour Protection as Surface Load

In the second case the scour protection is modelled as surface load to investigate the effect of the surcharge load on the stiffness of soil surrounding the pile. The surcharge load is equal to the weight of the purposed scour protection layer with properties as described in table 3.4. This case is also divided into 5 load steps as described in section 3.3.3.

3.4.3 Scour Protection as Dedicated Layer

In the final case the scour protection is modelled as a layer on top of the subsoil with properties as described in table 3.4. This case is also divided into 5 load steps as described in section 3.3.3.

Results from Simulations

This chapter presents the results from simulations of a monopile placed in Hokksund sand done with 3D FEM software Plaxis. The model used in the simulations is according to chapter 3. The resulting bending moment from the simulations have been used to calculate soil response and p-y curves for different depths along the pile. The simulations have been divided into three cases; pile only, pile with surface load and pile with scour protection layer. The results from the simulations have been post-processed in Excel and MatLab.

4.1 Bending Moment and Soil Response from Simulations

As described in section 3.3.1 the bending moment is obtained by including a soft beam in the centre of the pile. Plaxis includes built in tools to generate bending moment distributions for beams. The results from the simulations is divided into three different cases as described in section 3.4.

Calculating soil response from bending moment

After obtaining the bending moment, the soil response can be calculated with the following equation:

$$P(z) = \frac{d^2 M(z)}{dz^2} \quad (4.1)$$

Where:

P: soil response

M: bending moment

z: depth

When the soil response is known it is possible to extract the lateral deflection from the soft beam using built in tools on Plaxis. The general calculation procedure is described in figure 4.2.

The moment from the soft beam can be scaled up to represent the moment for the whole pile. To do this the equivalent Young's modulus and the moment of inertia is needed for both the soft beam and the pile.

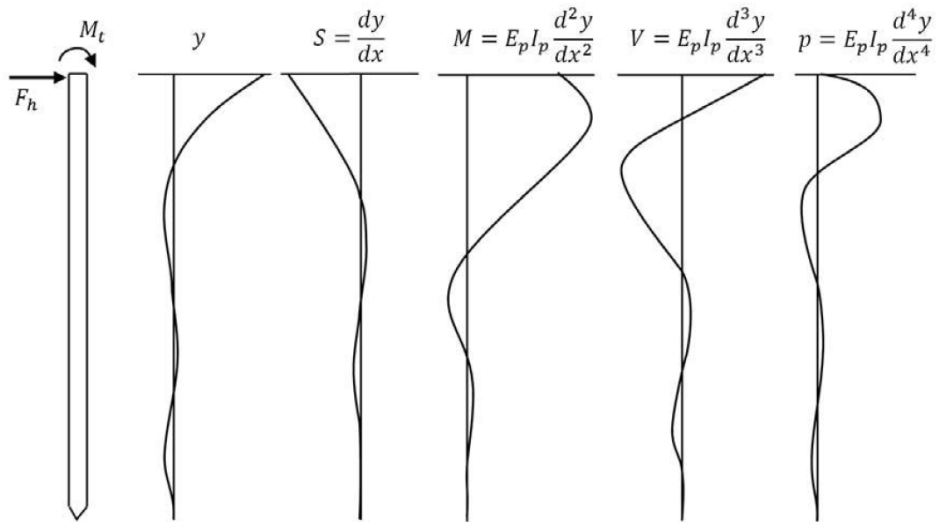


Figure 4.1: Derivatives of the 4th order beam equation, from Hanssen (2016).

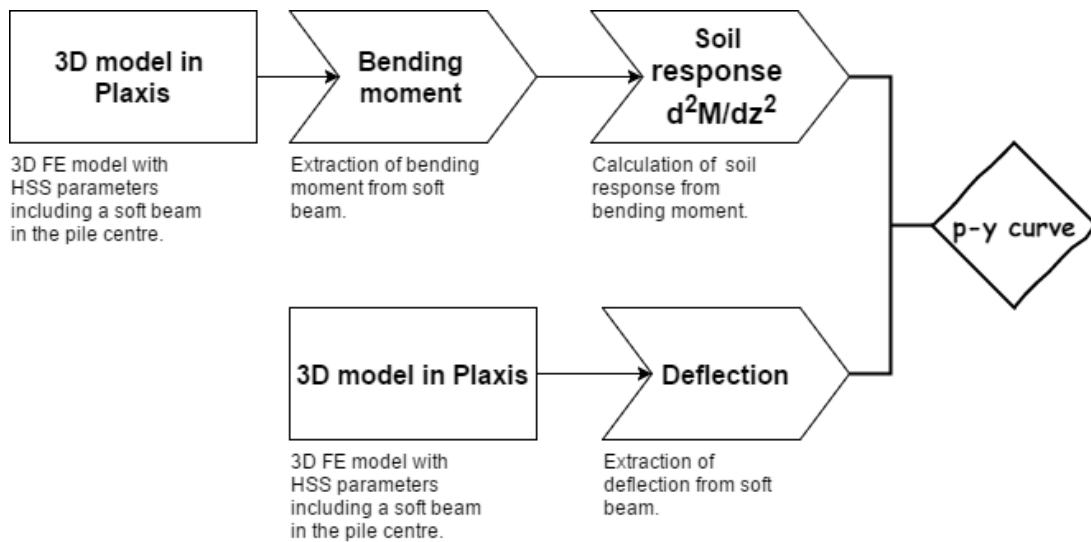


Figure 4.2: Flow chart of calculation procedure for p-y curves from Plaxis.

The soft beam is given as:

$$EI = 1$$

The moment of inertia for a pile with radius r and wall thickness t is given as:

$$I = \frac{\pi}{4} \left(r^4 - (r - t)^4 \right) \quad (4.2)$$

The moment of inertia for a cylinder is given as:

$$I_{cyl} = \frac{\pi}{4} r^4 \quad (4.3)$$

The moment is generally given as:

$$M = EI \frac{d^2 y}{dx^2} \quad (4.4)$$

To find the equivalent moment in the pile the moment from the beam must be multiplied with EI/EI_{beam} :

$$\begin{aligned} E_{steel} &= 210 \text{ GPa} \\ I &= \frac{\pi}{4} \left(3^4 - (3 - 0,08)^4 \right) \\ &= 6,52 \text{ m}^4 \\ \frac{EI}{EI_{beam}} &= \frac{210.000.000 \text{ kPa} \cdot 6,52}{1} \\ &= 13,69 \cdot 10^8 \end{aligned}$$

With the equivalent Young's modulus for the pile with volume elements the result should be the same as for the original hollow pile:

$$\begin{aligned} E_{equ} &= 210 \cdot 10^8 \left(1 - \left(\frac{3 - 0,08}{3} \right)^4 \right) = 21.500.000 \text{ kPa} \\ I_{cyl} &= \frac{\pi}{4} 3^4 \\ &= 63,6 \text{ m}^4 \\ \frac{EI_{equ}}{EI_{beam}} &= \frac{21.500.000 \text{ kPa} \cdot 63,6}{1} \\ &= 13,68 \cdot 10^8 \end{aligned}$$

The formulations seem to fit well. After correcting the moment from Plaxis the soil response can be calculated with eq. 4.1.

The soil response can also be shown by investigating the normal stress on the interface elements around the pile in Plaxis. When the soil response $p(z)$ and the lateral deflection $y(z)$ is known for a given load step and depth, a point in the $P(z)$ - $y(z)$ curve can be constructed. By simulation different load steps a full p - y curve for a given depth can be constructed.

4.1.1 Results from Case Without Scour Protection

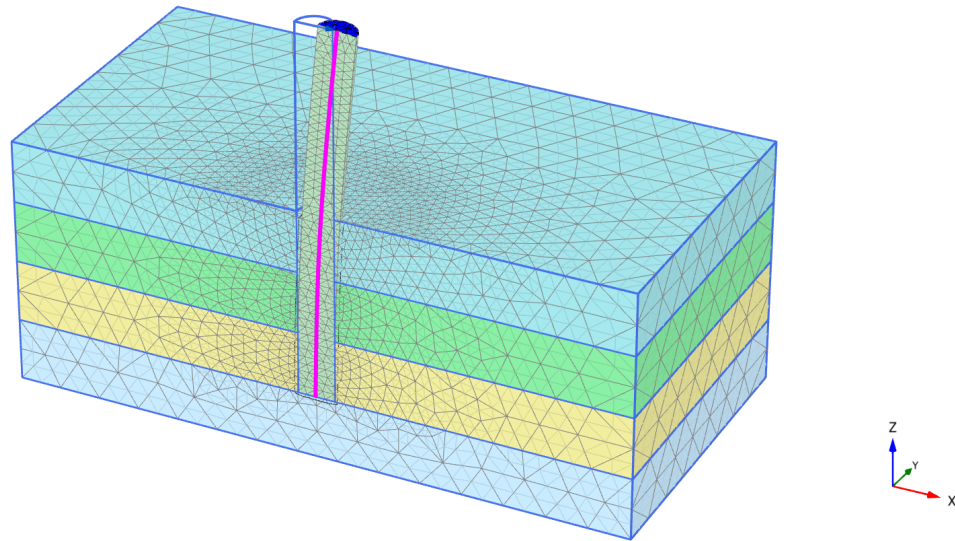


Figure 4.3: Model from Plaxis with no scour protection and load of 5000 kN.

Figure 4.3 shows a deformed mesh figure from Plaxis illustrating the pile when it's exposed to a horizontal load of 5000 kN at the top of the pile. In this model there is no surface load or scour protection layer. The moment distribution and soil response along the pile for a horizontal load of 1000 kN, 2000 kN and 5000 kN is shown in figure 4.4. The moment increases linearly from the top of the pile down to the top of the soil. At the top of the pile there is some distortion due to the horizontal load and the plate element on the top. The moment at the top of the soil should be equal to the load times the moment arm, around 150 MNm for load of 5000 kN. This seems to correlate well. The soil response should be zero above the soil, but due to the load and plate at the top there is some distortion also here. For further calculations this does not effect the results, as only the embedded length of the pile is used to calculate p-y curves. The bending moment and corresponding normal stress on the interface elements is shown in figure 4.5 - 4.6.

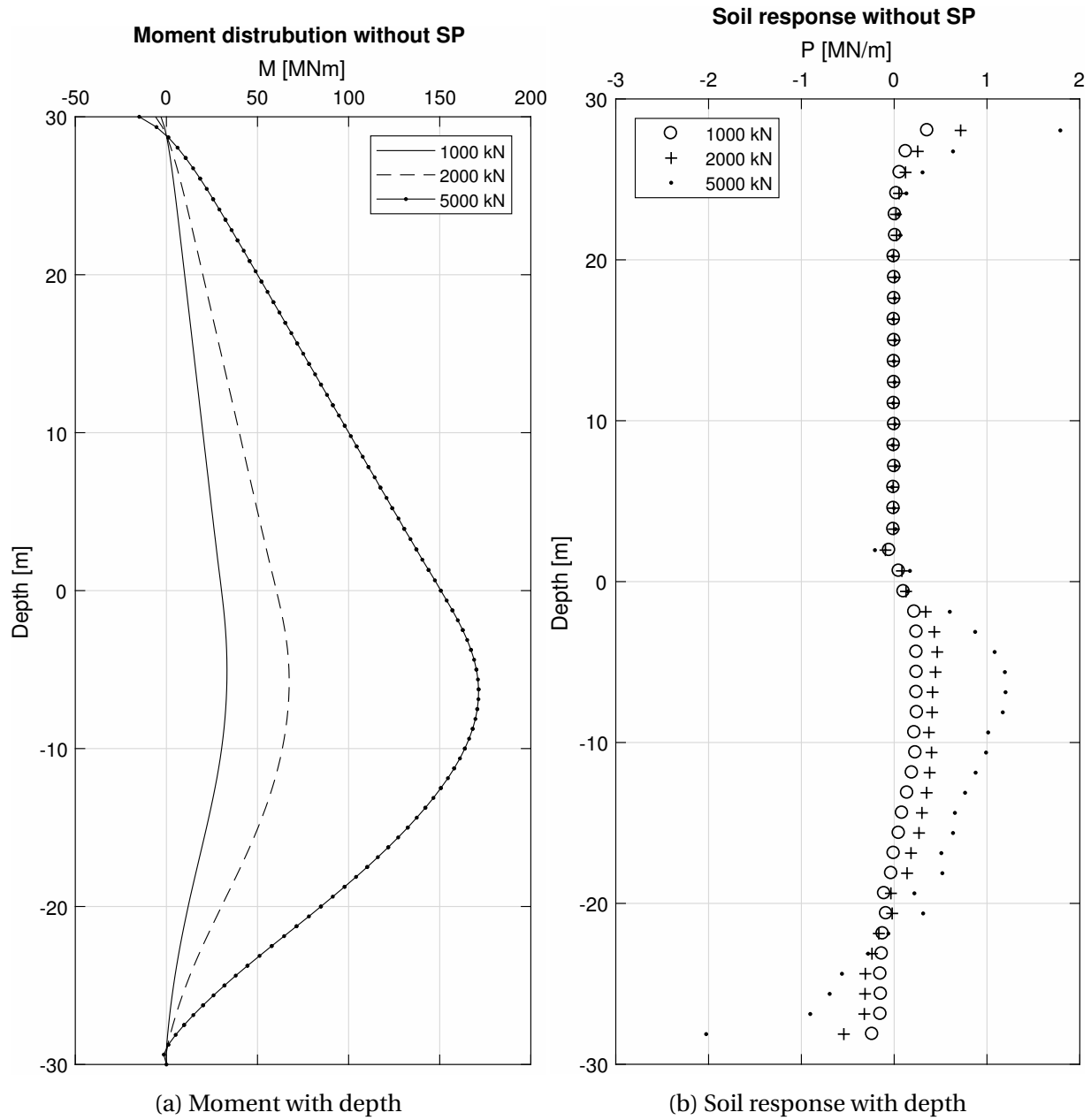


Figure 4.4: Moment and soil response with depth for case with no scour protection.

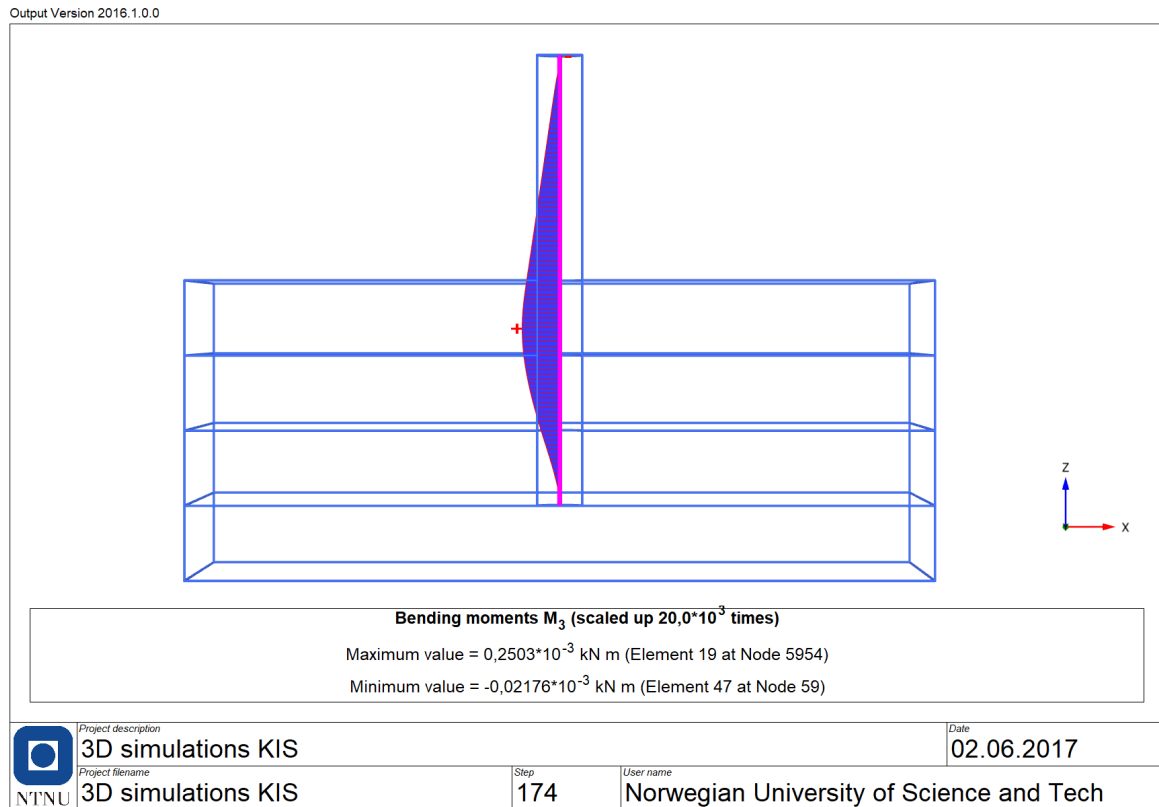


Figure 4.5: Moment distribution from Plaxis along beam for case without scour protection at load step 5000 kN

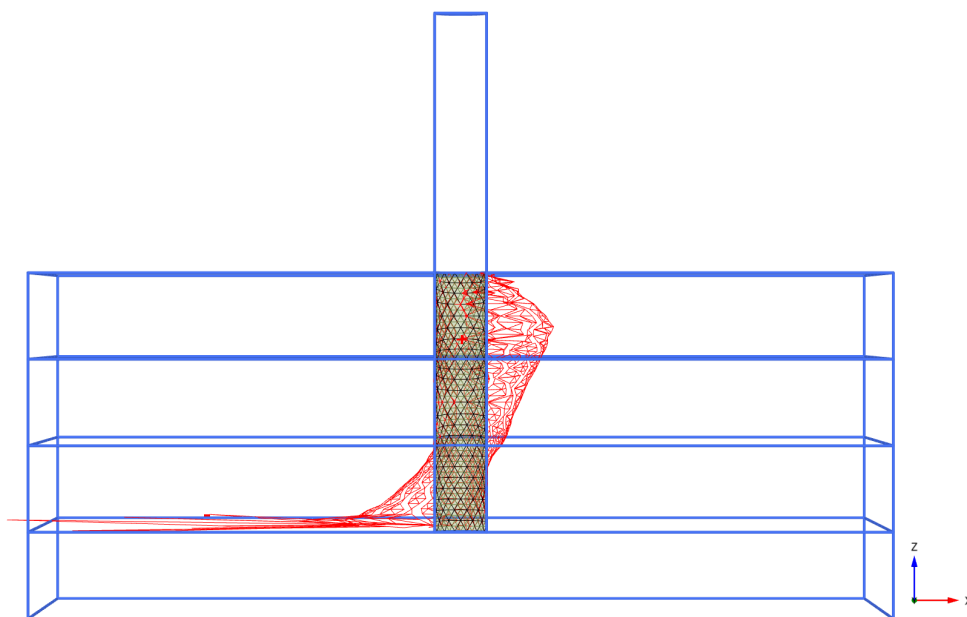


Figure 4.6: Interface stress for case without scour protection at load step 5000 kN.

4.1.2 Results from Case With Surface Load

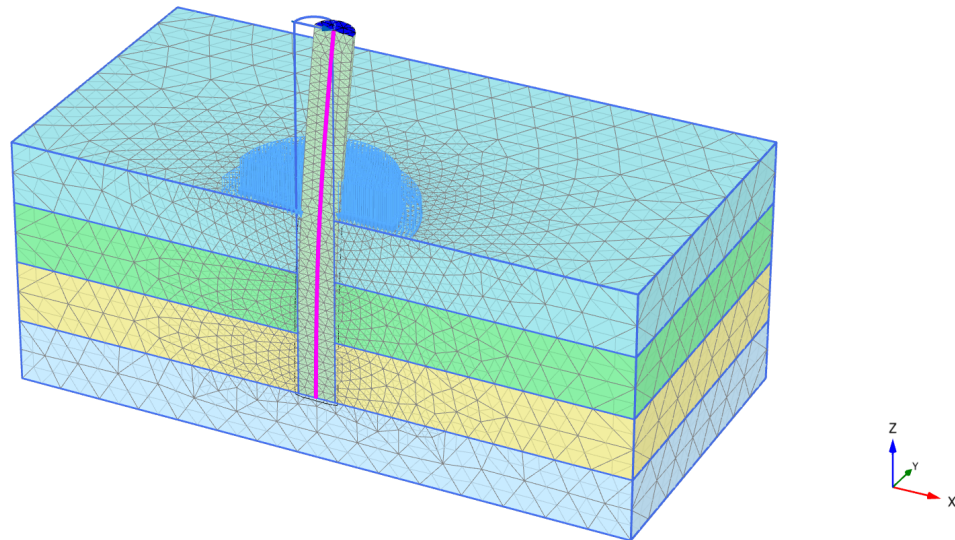


Figure 4.7: Model from Plaxis with surface load and load of 5000 kN.

Figure 4.7 shows a deformed mesh figure from Plaxis illustrating the pile when it is exposed to a horizontal load of 5000 kN in the top of the pile. In this model there is a surface load corresponding to the weight of a scour protection layer. The moment distribution and soil response along the pile for a horizontal load of 1000 kN, 2000 kN and 5000 kN is shown in figure 4.8. Also here the moment increases linearly from the top of the pile down to the soil. The distortions in moment and soil response is present also here, but again only the embedded length of the pile is used to calculate p-y curves. The bending moment and corresponding normal stress on the interface elements is shown in figure 4.9 - 4.10.

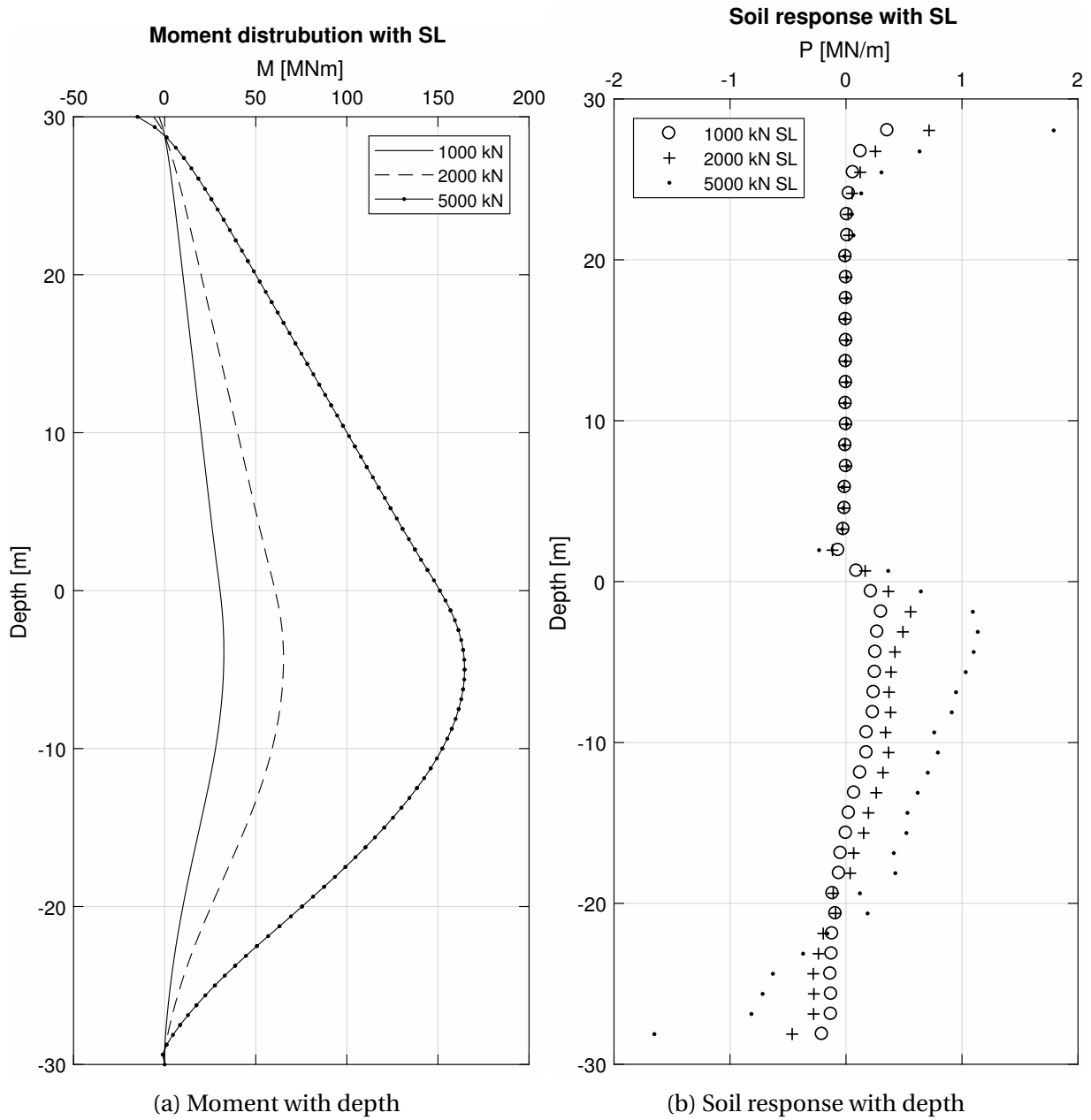


Figure 4.8: Moment and soil response with depth for case with surface load.

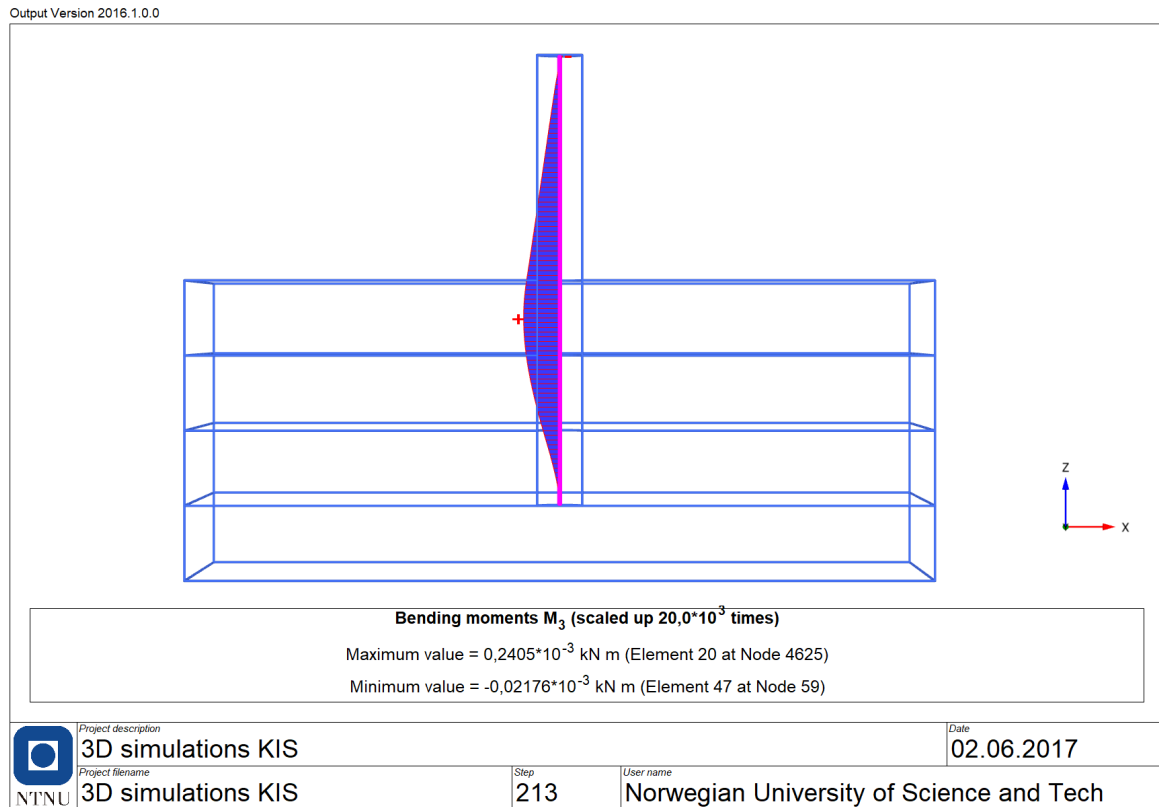


Figure 4.9: Moment distribution from Plaxis along beam for case with surface load at load step 5000 kN

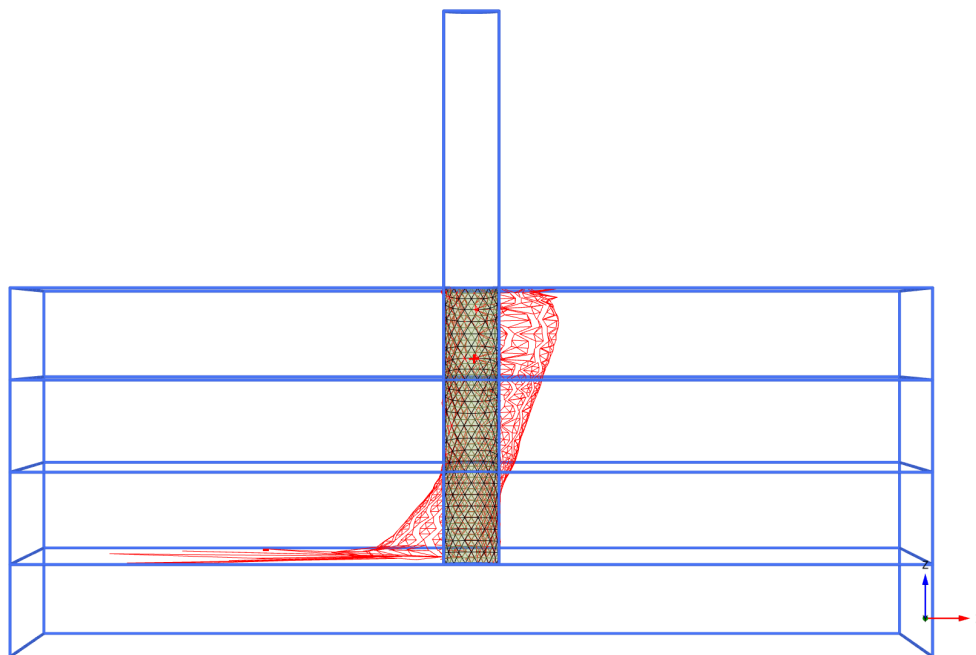


Figure 4.10: Interface stress for case with surface load at load step 5000 kN.

4.1.3 Results from Case With Scour Protection Layer

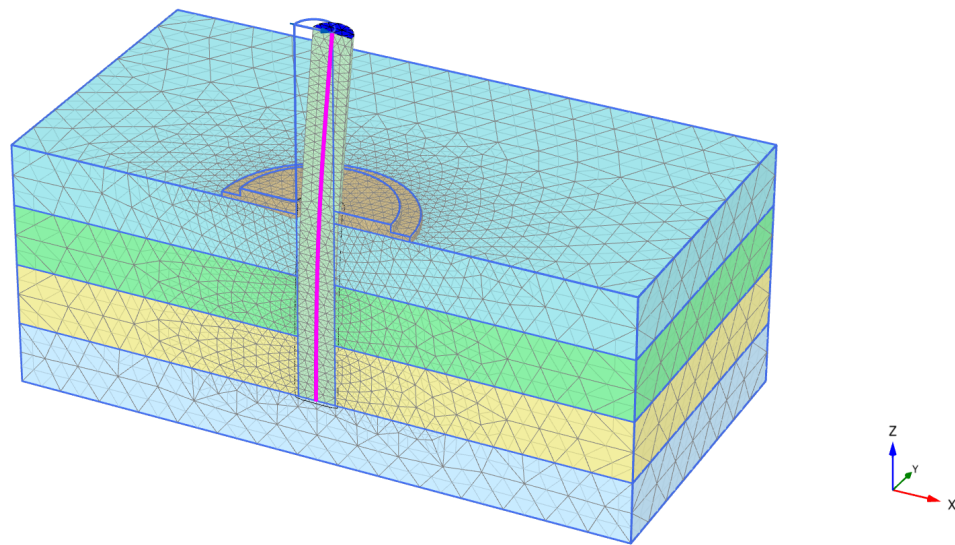


Figure 4.11: Model from Plaxis with scour protection layer and load of 5000 kN.

Figure 4.11 shows a deformed mesh figure from Plaxis illustrating the pile when it is exposed to a horizontal load of 5000 kN at the top of the pile. In this model there is a scour protection layer around the pile with properties as described in table 3.4. The moment distribution and soil response along the pile for a horizontal load of 1000 kN, 2000 kN and 5000 kN is shown in figure 4.12. The moment and soil response show the same behaviour as in the previous cases, but the linear part of the moment distribution seems to stop a bit higher than in the previous cases. This fits well with the presence of the SP layer on top of the soil. There is also a soil response above the soil which indicates that the SP layer responds to the lateral pressure from the pile. The bending moment and corresponding normal stress on the interface elements is shown in figure 4.13 - 4.14.

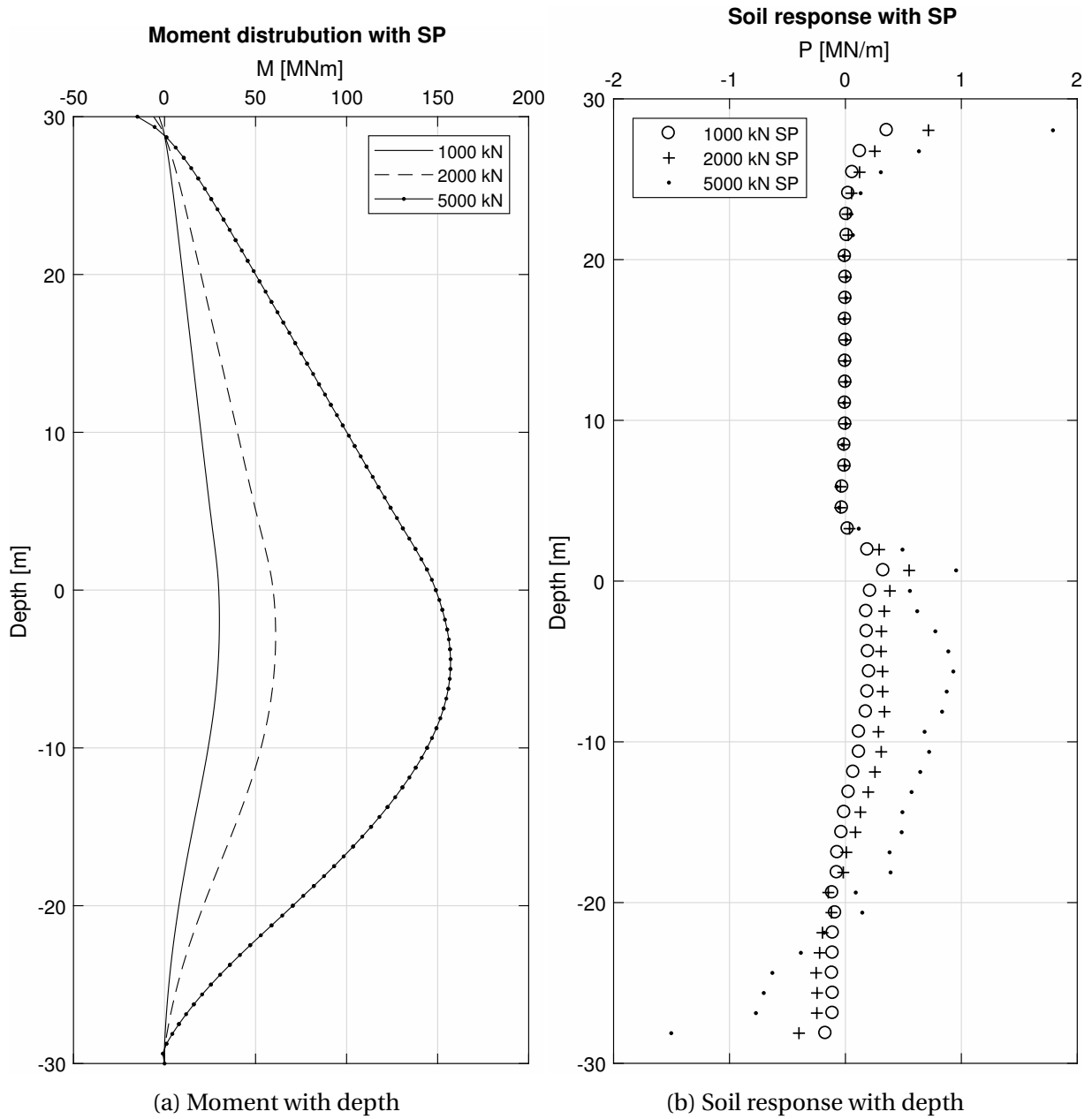


Figure 4.12: Moment and soil response with depth for case with scour protection layer.

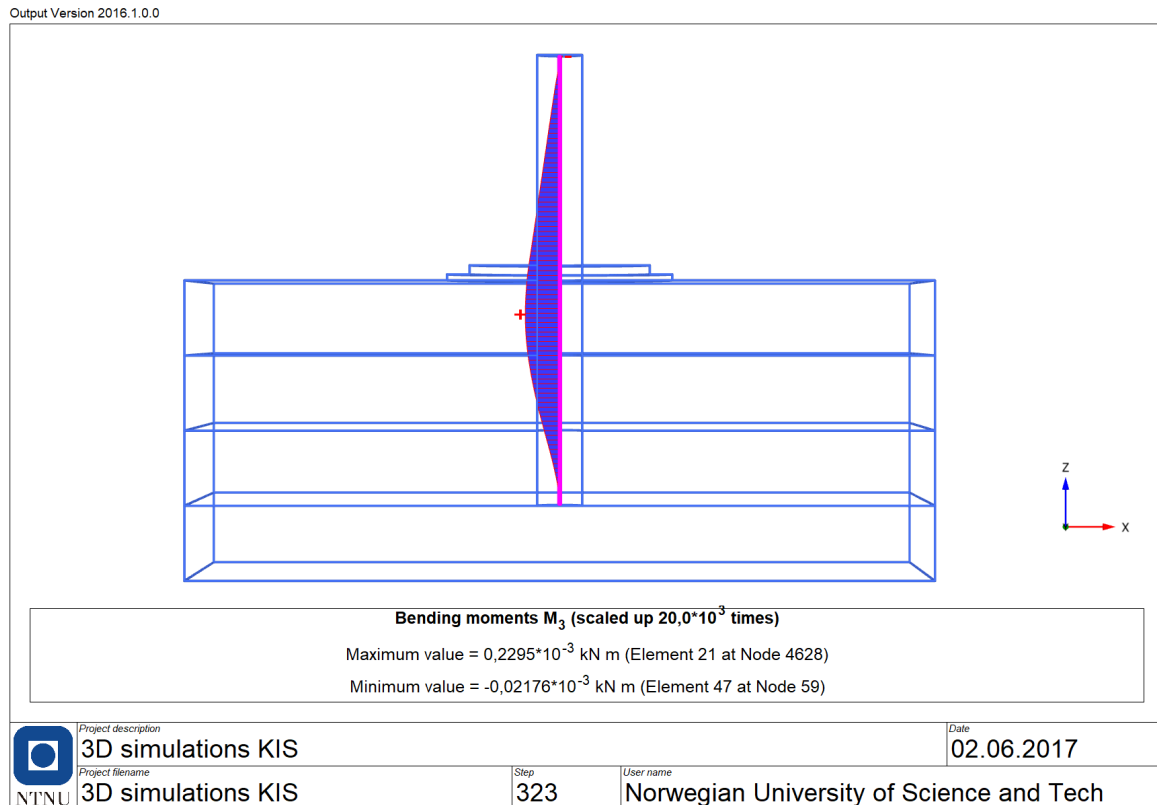


Figure 4.13: Moment distribution from Plaxis along beam for case with scour protection at load step 5000 kN

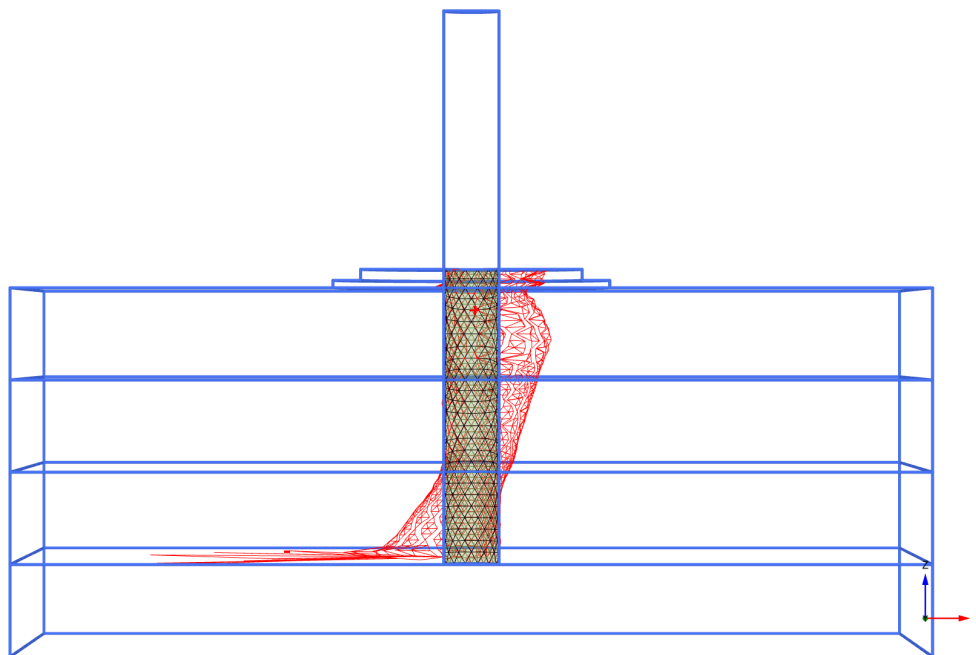


Figure 4.14: Interface stress for case with scour protection layer at load step 5000 kN.

4.2 Lateral Deflection from Simulations

The lateral deflection of the soil can be found by extracting the lateral displacement of the centre beam in the x-direction from Plaxis.

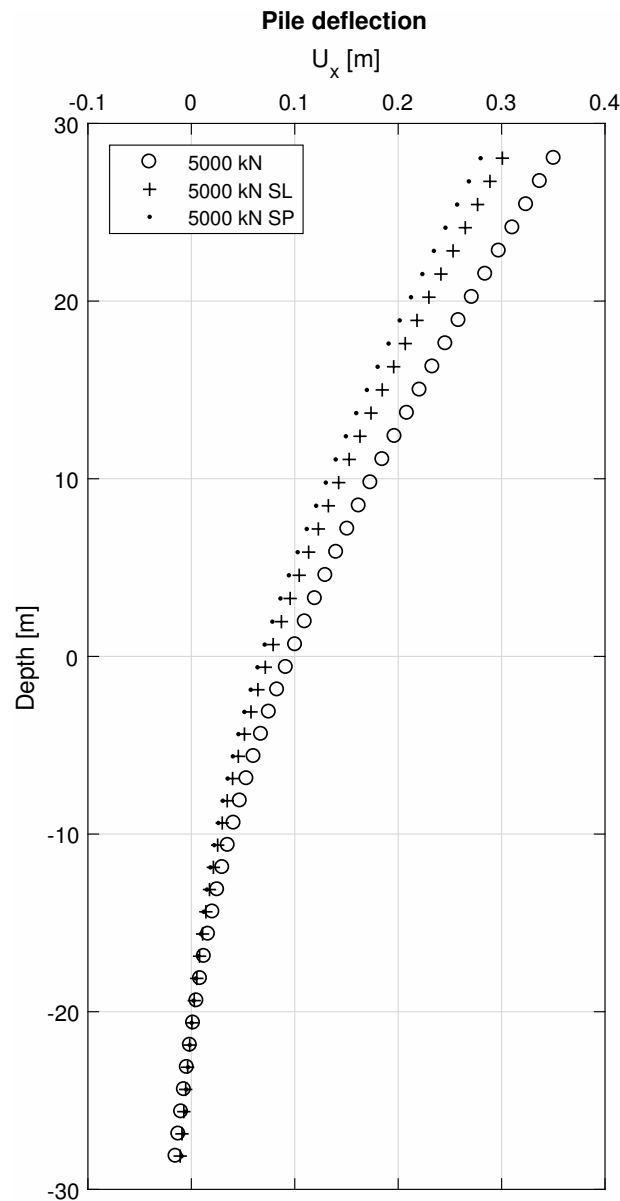


Figure 4.15: Pile deflection at 5000 kN for all cases.

Figure 4.15 presents the pile deflection at 5000 kN for the different cases. For the calculation of p-y curves the deflection for all load steps is included. The figure shows a clear effect of both surcharge load and the scour protection layer on the deflection of the pile. The difference between the deflection with surcharge load and scour protection layer implies that the scour protection layer has an effect beyond the pure effect of surcharge load. Figure 4.15 also shows that the pile rotates near the bottom, around -20 m, but with small difference between the cases.

4.3 Calculation of p-y curves from Simulations

The p-y curves can be calculated by plotting the soil response $p(x)$ against lateral deflection $y(x)$ for different load steps at different depths.

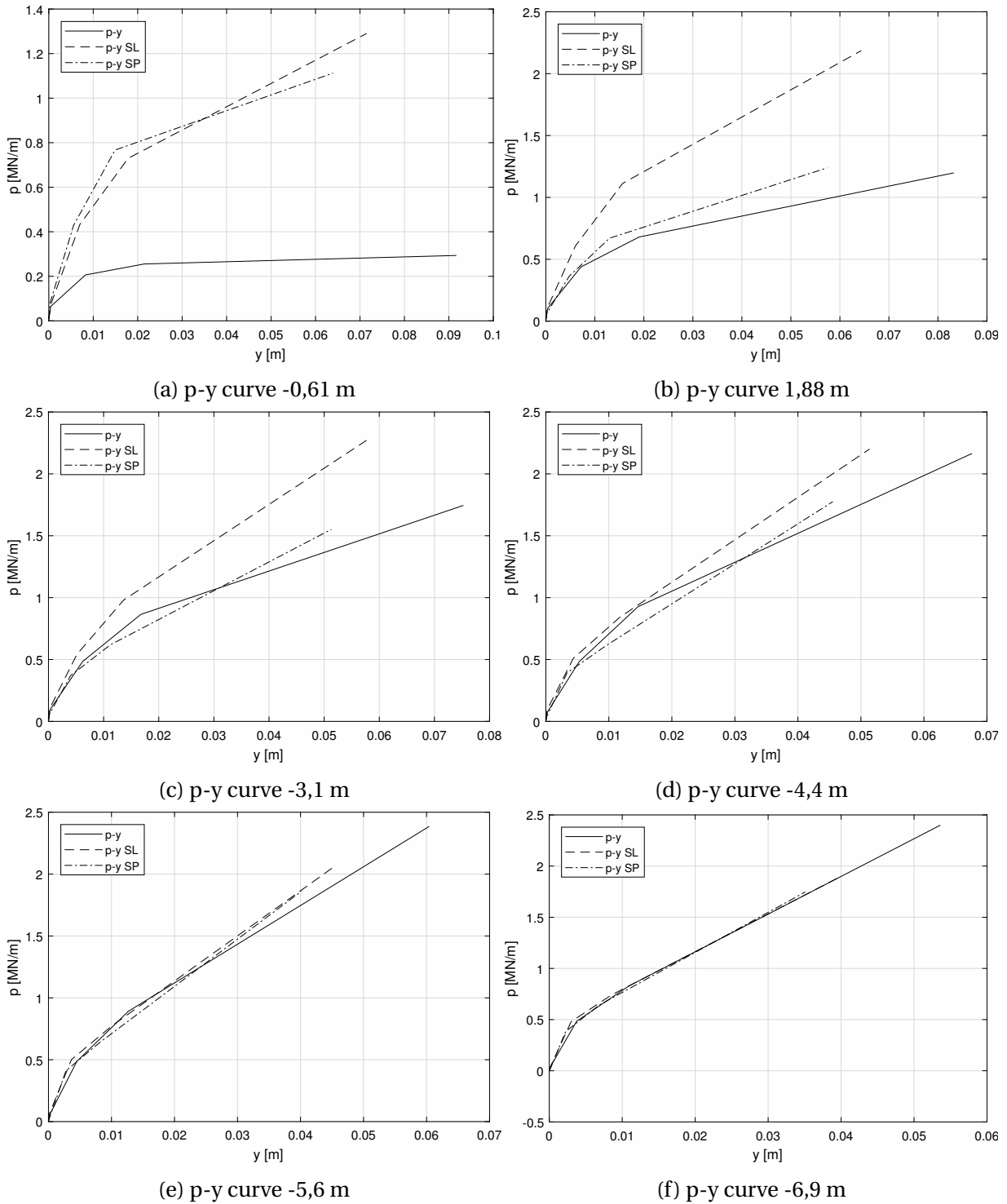


Figure 4.16: p-y curves from -0,61 to -14,4 m.

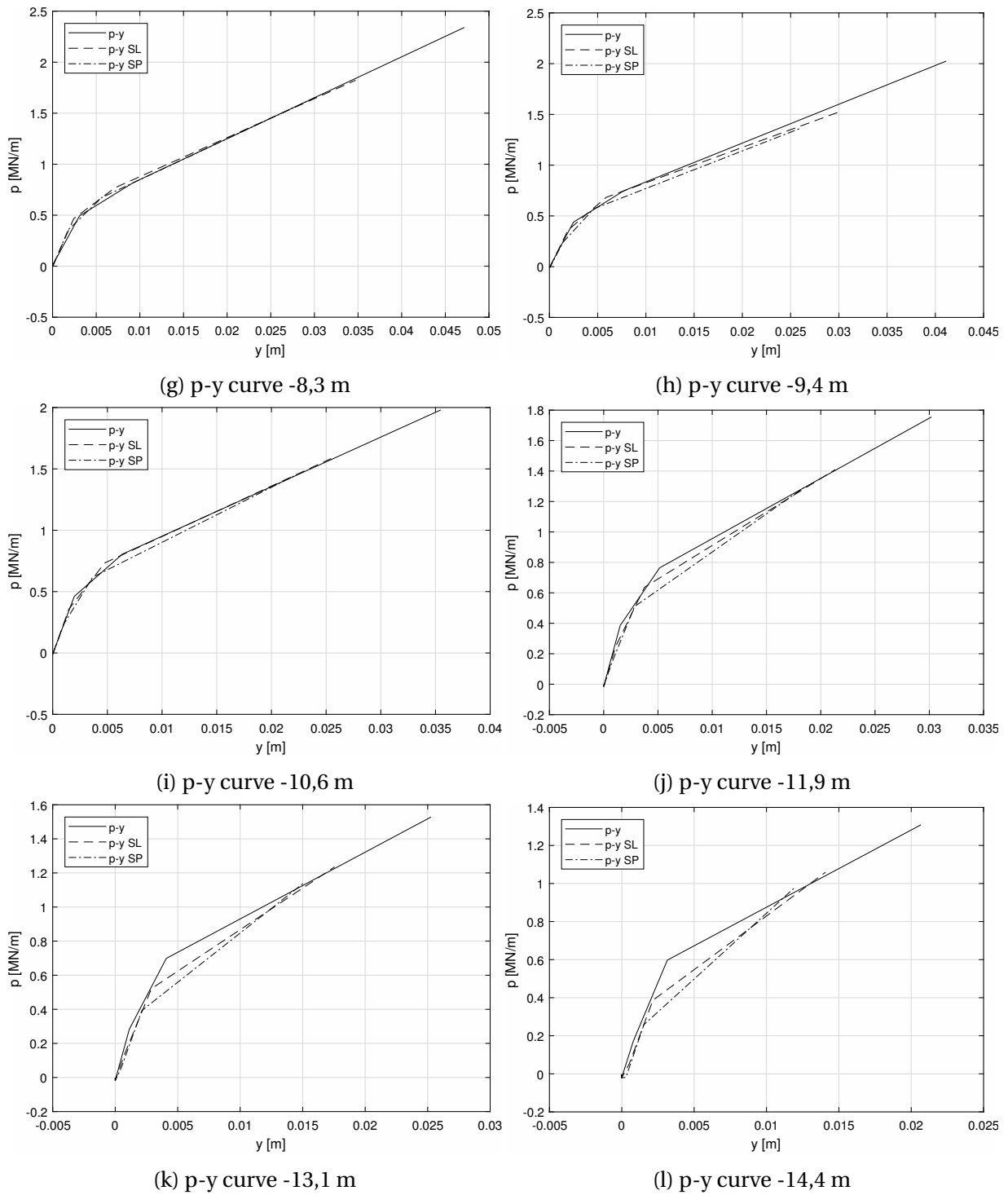


Figure 4.16: p-y curves from -0,61 to -14,4 m cont.

The p-y curves for depth down to -14,4 m is plotted in figure 4.16. Close to the rotation point of the pile the results are ambiguous. This is due to the fact that when the pile rotates it pushes the soil, so there will be areas with pressure and no displacement and displacement without pressure. From figure 4.4, 4.8 and 4.12 the rotation point seems to be around -20 m. In order to get reliable results the depth from -14,4 to -23,1 is disregarded (1D over rotation point and 0,5D below rotation point).

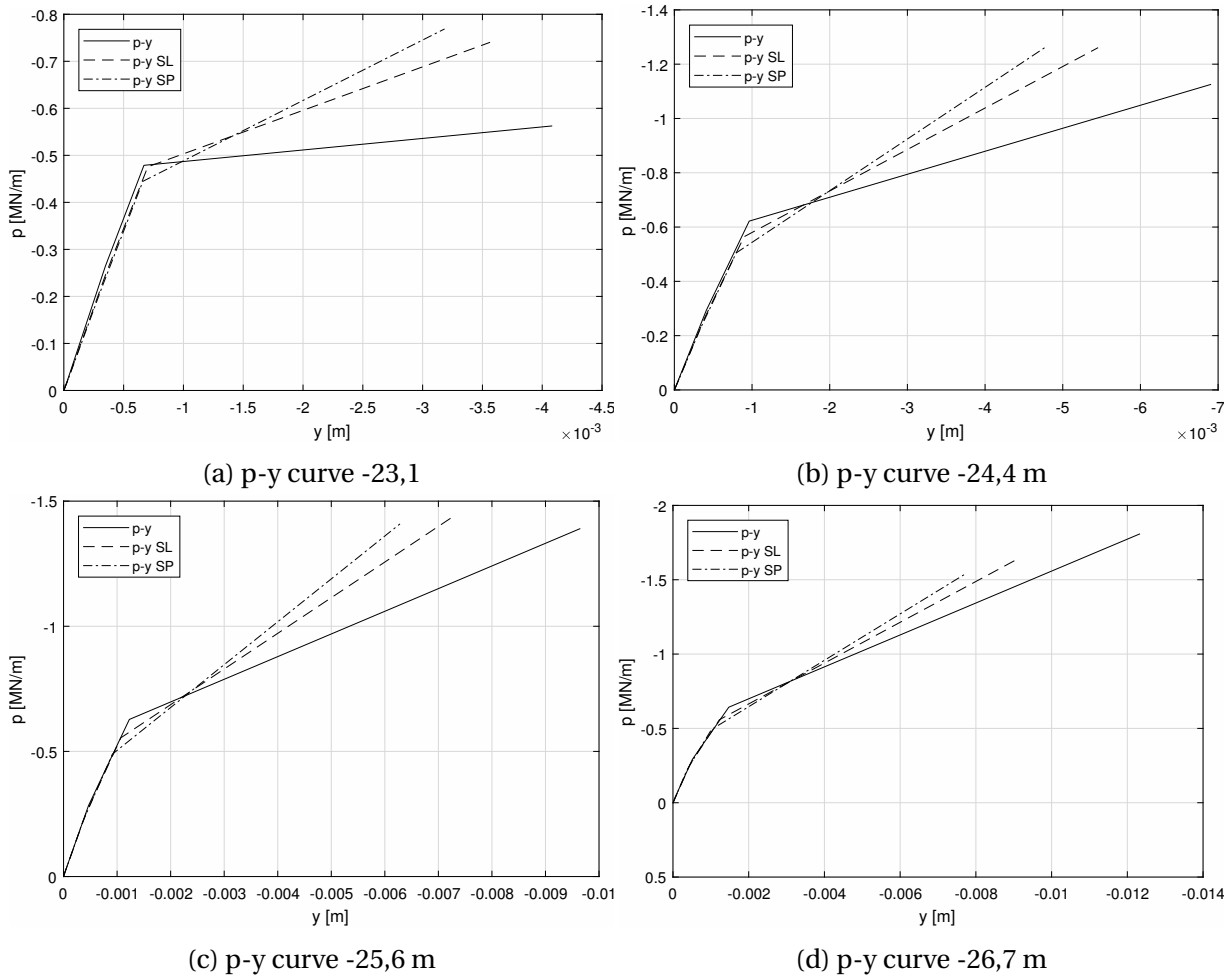


Figure 4.17: p-y curves from -23,1 to -26,7 m.

Figure 4.17 presents the p-y curves below the rotation point from -23,1 m to -26,7 m. The area beneath -26,7 is disregarded due to ambiguity in the results at the end due to the rotation of the pile (toe-kick). The negative axis values means that the stress and strain is in the opposite direction compared to the values above the rotation point.

Discussion

The main objective of this thesis is to evaluate the effect of scour protection on the lateral stiffness/response of a monopile foundation. To assess the effect simulations with 3D-FEM software Plaxis have been done with a real size model placed in a sand material similar to the model sand used at NTNU. Simulations has been divided in to three cases to adequately evaluate the effect of the scour protection. In chapter 6 the results from the simulations is presented. This chapter will discuss the results of the simulations and compares the three different cases used in this study.

5.1 Comparison of Results

The results for all cases show a clear effect of both the surcharge load and the scour protection layer itself. From the lateral deflection it is clear that the lateral behaviour of the pile is effected by the soils increased stiffness caused by the surcharge load and the scour protection layer. In figure 5.1 the moment distribution and soil response for the load-step of 5000 kN for all cases is presented.

Figure 5.1 shows a clear reduction of the moment along the pile as well as an increase in the soil response down to a depth of $Z < D$ and lowering of the soil response deeper than $Z > D$. Around the rotation point of the pile (~ 20 m) it is hard to assess the soil response because when the pile rotate it push on the soil so there will be pressure without displacement and displacement without pressure and this will not yield any results. The soil response in this part of the pile can be interpolated between the upper and lower areas where there is reliable results.

5.1.1 Change in p-y Curves

P-y curves for different depths and cases i presented in section 4.3. The curve are based on the calculated soil response and lateral deflection from moment distribution along the pile. From the curves it is clear that the scour protection has a substantial influence on the stiffness of the upper layers of the soil. Both the SL and SP cases show an increase in the soil response in the upper 3-4 m. Further down is seems that the effect decreases and the p-y curves is coinciding. This can be explained by stress distribution theory where the effect of a surcharge load decreases both with depth and horizontal distance from the load.

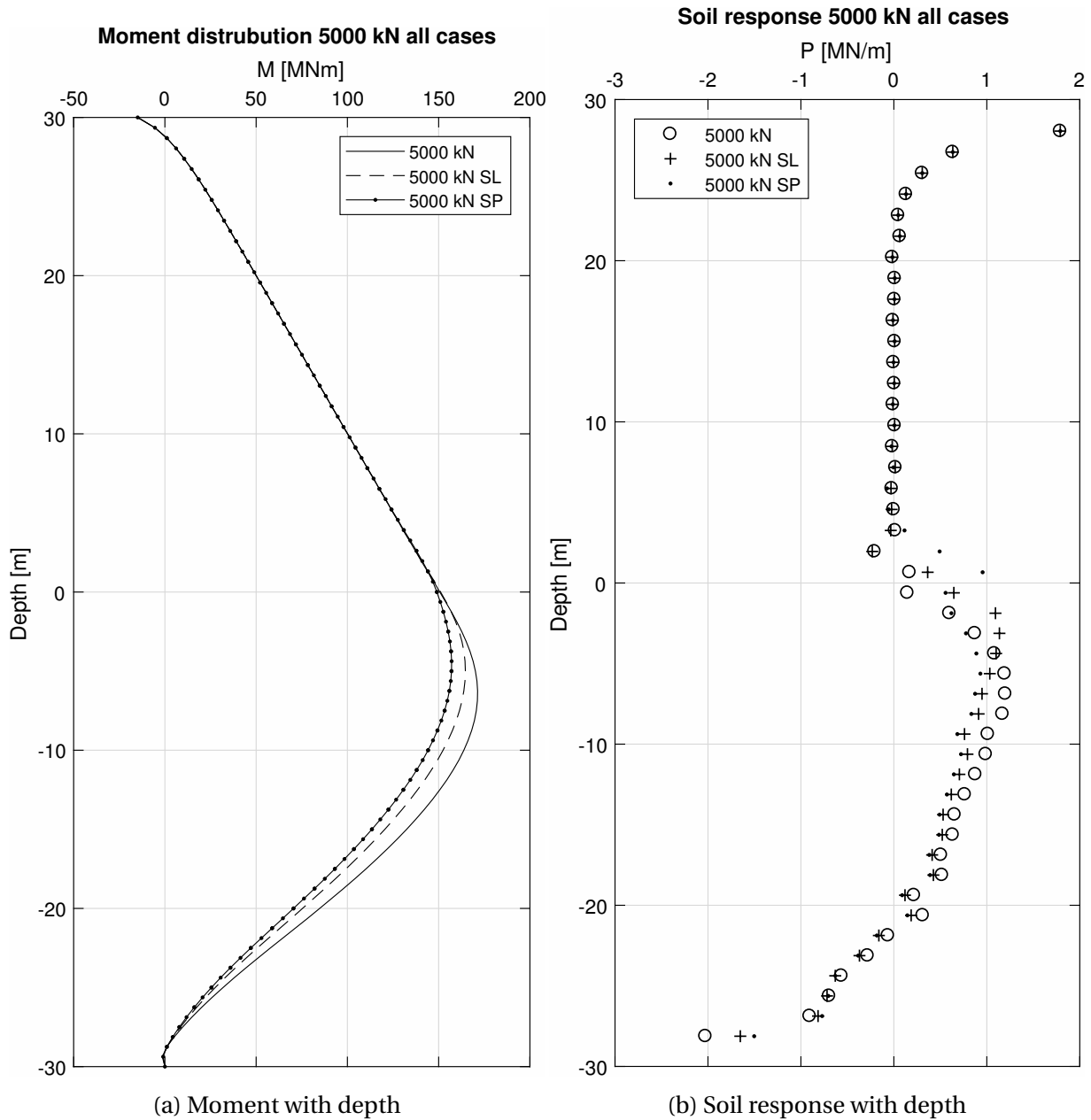


Figure 5.1: Moment and soil response with depth for a load of 5000 kN for all cases.

Comparison with API

As described in section 2.4.1 the design codes by DNV (2014); API (2011) describes formulations for developing p-y curves for different ground conditions. To compare the results from Plaxis it is made p-y curves for the case without scour protection.

Figure 5.2 shows the p-y curves based on the API formulation from section 2.4.1 with deflection corresponding to the results from Plaxis simulations without scour protection. The figure show a general increase in stiffness with depth and that the lower levels still is in the elastic range when exposed to the 5000 kN load step.

Figure 5.3 compares the p-y curves from API and Plaxis. From the figure it seems that the shallow levels correlates well with the API formulations, but with depth API seems to overestimate the stiffness. The Plaxis graphs from -0,36 m, -1,88 m and -3,12 m fits well with the

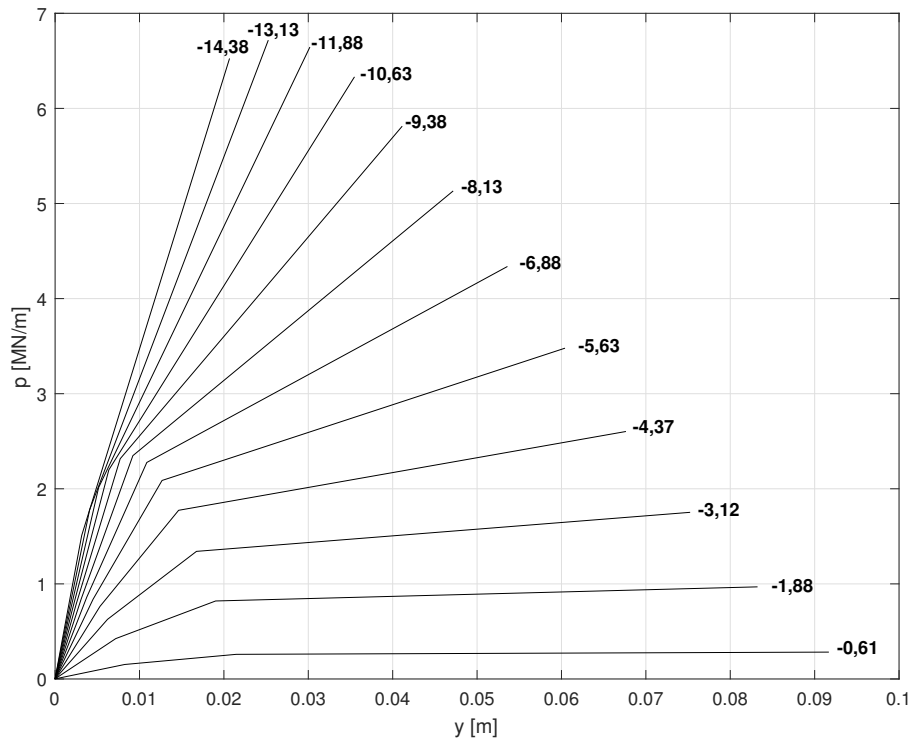


Figure 5.2: p-y curves based on API formulation for case without scour protection.

API results, but API seems to give higher initial stiffness. This is due to the linear increase in stiffness with depth in the API formulations. The soil model in Plaxis (HSS) designed to have a parabolic increase in stiffness with depth. This results in API overestimating the stiffness at larger depths.

Figure 5.4 is a closer plot of figure 5.3 in the small strain are. From the figure it seems that the soil response is similar but HSS gives a much higher stiffness with deflection below 0,001 m for the upper layers of the soil. Also the linear-elastic, perfectly plastic approach idealisation in the API formulation of p-y curves differs from the parabolic gradual decrease in stiffness in the HSS formulation, resulting in the difference in the development of the curves with deflection as shown in figure 5.3.

5.2 Change in Eigenfrequency

The eigenfrequency of a offshore wind turbine is an important design driver, the eigenfrequency can be calculated from the secant stiffness extracted from the p-y curves used in a Winkler foundation model.

$$f[sec] = \frac{1}{2\pi} \sqrt{\frac{k_s}{M}} \quad (5.1)$$

Where:

k_s : force/displacement at top of pile

M: top mass

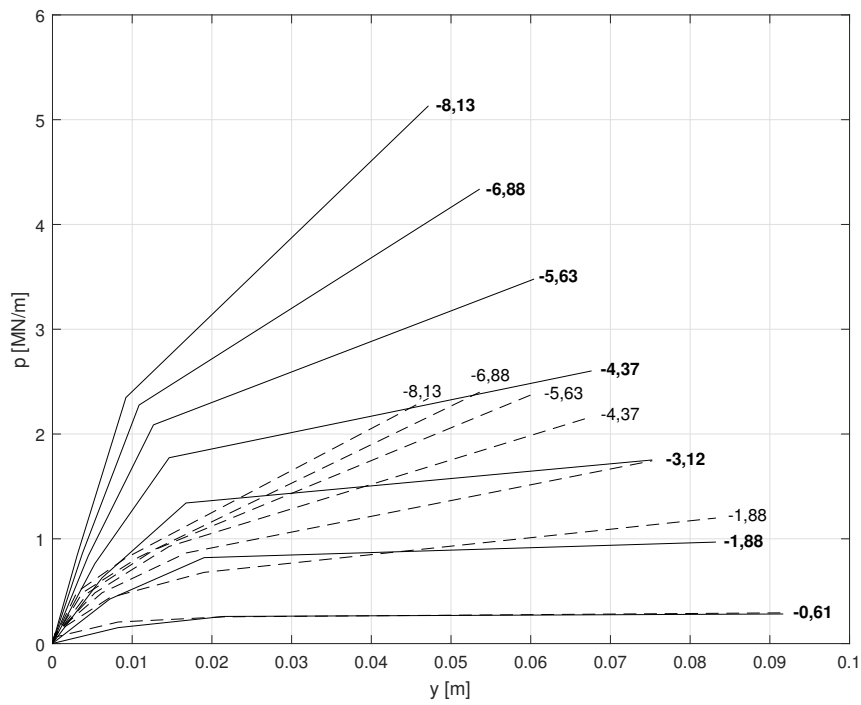


Figure 5.3: p-y curves based on API formulation (**bold text**) for case without scour protection compared with p-y curves from Plaxis.

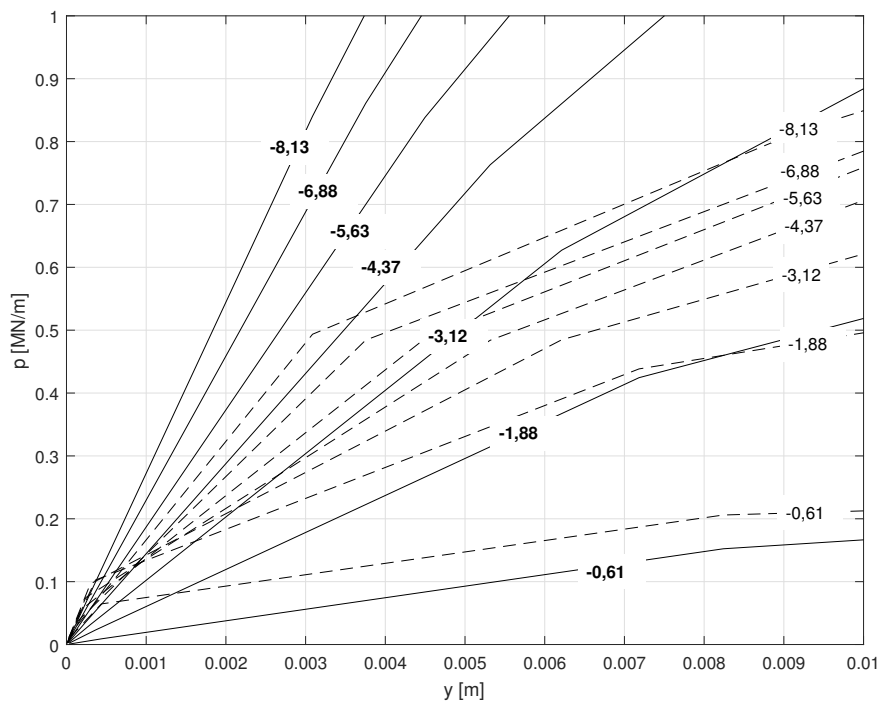


Figure 5.4: p-y curves in the small strain area based on API formulation (**bold text**) for case without scour protection compared with p-y curves from Plaxis.

Here the eigenfrequency is calculated using a simple 1-DOF approximation described by eq. 5.1. To calculate the eigenfrequency a mass is to be selected. The mass is selected to give a frequency of 0,3 sek. in the benchmark case with no scour protection and load step of 10 kN. The mass is kept constant for all cases and load steps. Eq. 5.1 is then used to calculate the corresponding frequency for SL and SP cases with the same mass. The mass can be found by rearranging eq. 5.1:

$$f = \frac{1}{2\pi} \cdot \frac{\sqrt{k_s}}{\sqrt{M}}$$

$$f \cdot \sqrt{M} = \frac{1}{2\pi} \cdot \sqrt{k_s}$$

$$\sqrt{M} = \frac{\sqrt{k_s}}{2\pi f}$$

$$M = \frac{k_s}{(2\pi f)^2}$$

For a target frequency of 0,3 sek. for load step of 10 kN in the benchmark case, the top mass was found to be $8,26 \cdot 10^6$ kg. This mass is used to calculate the eigenfrequency for all other cases and load step. Note that the top mass does not represent a full wind turbine, but only an example mass used to calculate the change in eigenfrequency for the different cases.

Table 5.1: Data used to calculate the frequency for all cases and load steps.

Data from Plaxis					
<i>Load step</i>	<i>10 kN</i>	<i>100 kN</i>	<i>1000 kN</i>	<i>2000kN</i>	<i>5000 kN</i>
Deflection at pile top [m]					
No SP	3,41E-04	3,63E-03	4,77E-02	1,08E-01	3,64E-01
SL	3,40E-04	3,55E-03	4,41E-02	9,83E-02	3,13E-01
SP	2,92E-04	2,99E-03	3,93E-02	8,90E-02	2,91E-01
Calculation of k_s [kN/m]					
No SP	2,93E+04	2,76E+04	2,09E+04	1,85E+04	1,37E+04
SL	2,94E+04	2,82E+04	2,27E+04	2,03E+04	1,60E+04
SP	3,43E+04	3,34E+04	2,55E+04	2,25E+04	1,72E+04
Calculation of f [sek]					
No SP	2,9609	2,8712	2,5021	2,3502	2,0261
SL	2,9656	2,9025	2,6030	2,4658	2,1858
SP	3,2011	3,1589	2,7586	2,5913	2,2656
Calculation of d_f [%]					
SL	0,16 %	1,09 %	4,03 %	4,92 %	7,88 %
SP	8,11 %	10,02 %	10,25 %	10,26 %	11,82 %

The results and intermediate results from frequency calculations is presented in table 5.1 and the results is shown in figure 5.5. Note that the values is for half of a pile. The change in eigenfrequency d_f is defined as $(f - f_0)/f_0$ where f_0 is the eigenfrequency from the benchmark case.

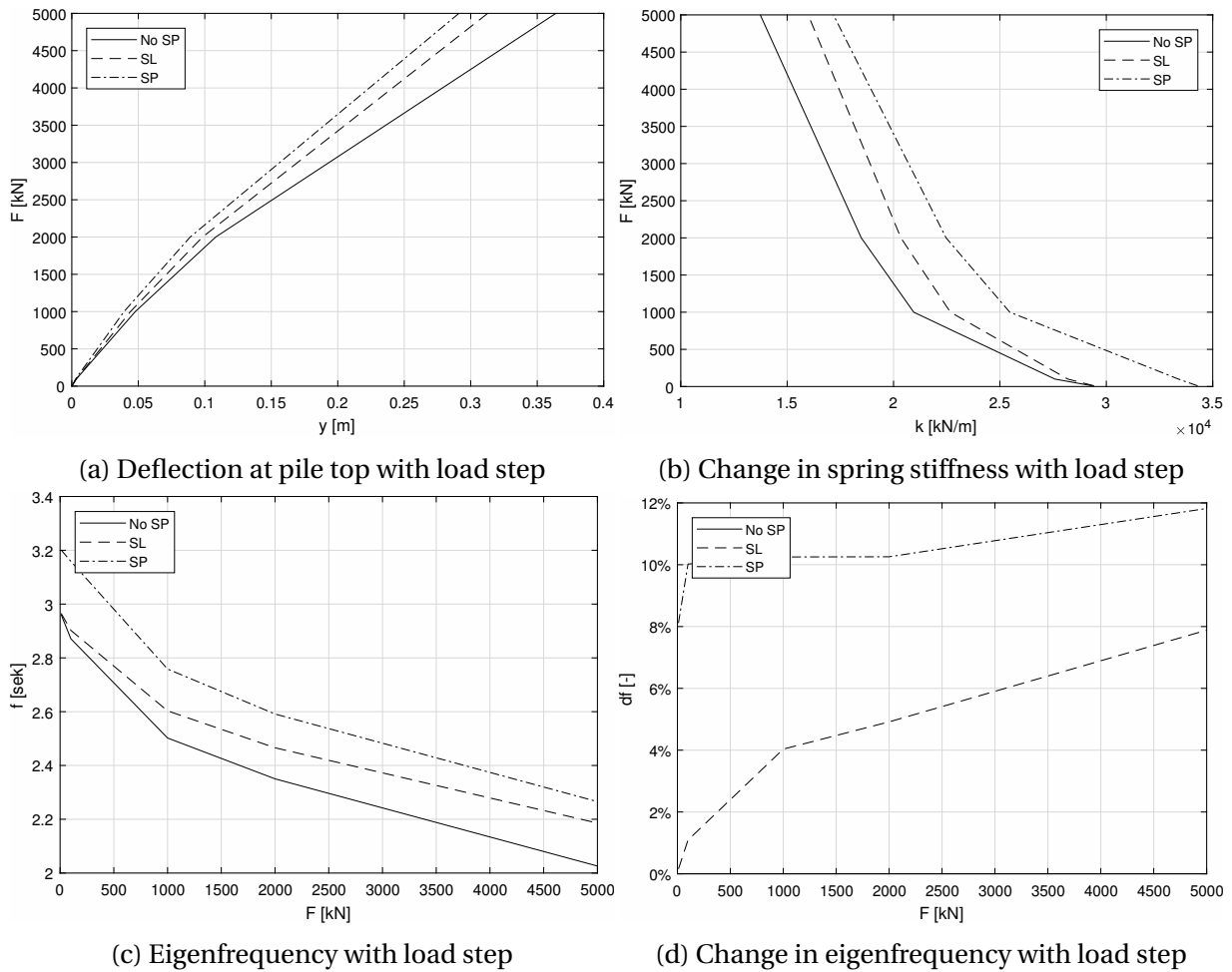


Figure 5.5: Change in eigenfrequency for a pile with mass on top.

Figure 5.5a shows the deflection at the pile top at different load steps. From the figure it is clear that both the surcharge load and the scour protection layer has an influence on the deflection of the pile. The deflection is then used to calculate the stiffness of the whole structure, where k_s is the force applied divided by the lateral deflection:

$$k_s = \frac{F[kN]}{y[m]} \quad (5.2)$$

Figure 5.5b show the change in k_s with different load steps. From the figure it seems that the spring stiffness is lower at higher lateral force. This correlates well with the p-y curves where the secant stiffness is lower at higher load steps, and the fact that the soil is stiffer in the small strain area. The figure also shows a difference between the different cases where the case with a scour protection layer gives the highest stiffness.

Figure 5.5c shows the change in eigenfrequency for the different load steps. Here the eigenfrequency for the case without scour protection is used as a benchmark case where the eigenfrequency is set to be $f = 0,3 \text{ sek}$. From the figure it is clear that the scour protection has an influence on the eigenfrequency of the structure, both as a surcharge load and an independent layer. In figure 5.5d the change in frequency is normalised to the benchmark case. From the figure it is clear that the scour protection gives a increase in eigenfrequency from about 1-10 % and the difference is highest in the biggest load steps.

5.2.1 Stiffness of Scour Protection Layer

The eigenfrequency is an important design driver, and deviation in the eigenfrequency compared to the designed value could lead to decreased lifetime of the structure due to fatigue or in worst case breakdown on the structure. Structural monitoring and back calculations on installed offshore wind turbines done by Kallehave (2015) have indicated that there is an deviation in the designed eigenfrequency from the measured eigenfrequency on site. Kallehave (2015) also did assessment on the stiffness of scour protection layer necessary to give the measured eigenfrequency and found the required stiffness to be from 200-350 MPa.

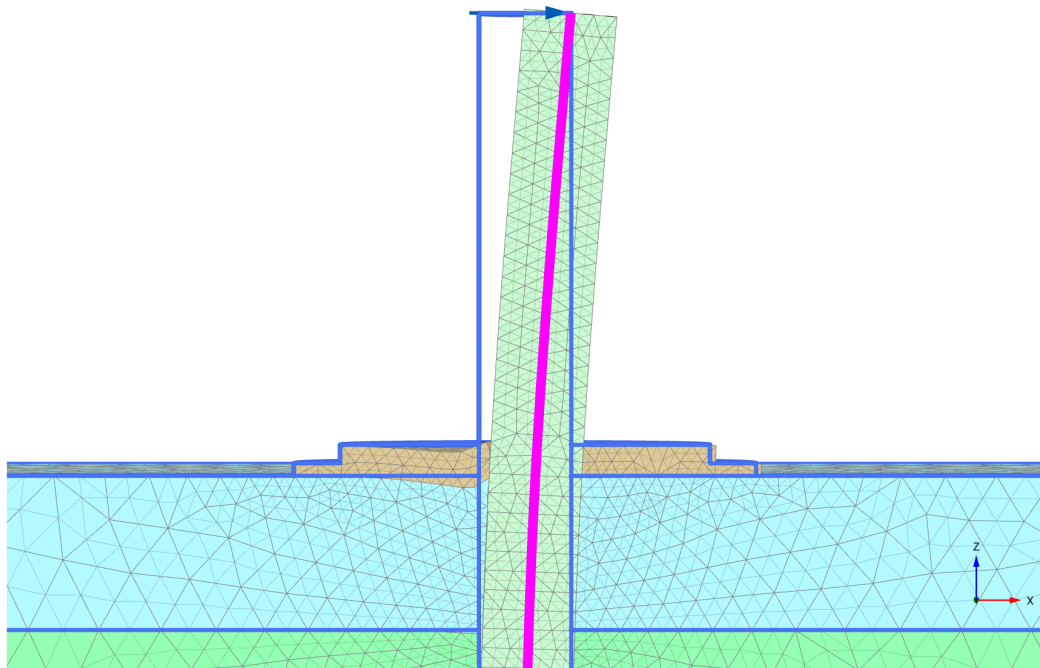


Figure 5.6: Deformation of scour protection layer with horizontal load of 5000 kN.

Figure 5.6 shows the deformed mesh of the pile with scour protection layer under a horizontal load of 5000 kN. From the figure it is clear that the SP is deformed under the pressure from the deflected pile, but the SP layer has also experienced lateral movement. In this thesis the SP layer have not been investigated in detail regarding the properties, but the result seems legitimate when considering large stone fills under lateral pressure. Some of the pressure leads to compaction of the stone fill, and some of the pressure is translated through the whole structure, and the shear strength of the stone fill - subsoil interface governs the lateral movement on the passive side of the pile. From figure 5.6 it also seems that gapping is occurring on the active side of the pile. This is also in accordance with observed soil behaviour

when large lateral deflection is occurring, e.g. storm events. Measurements done by Kallehave (2015) shows a drop in eigenfrequency after storm events, likely due to gaping between the pile and SP and/or subsoil. The observed drop in eigenfrequency is temporary, so the effect of the gap is reduced over time as the SP and subsoil is again settling in to the pile.

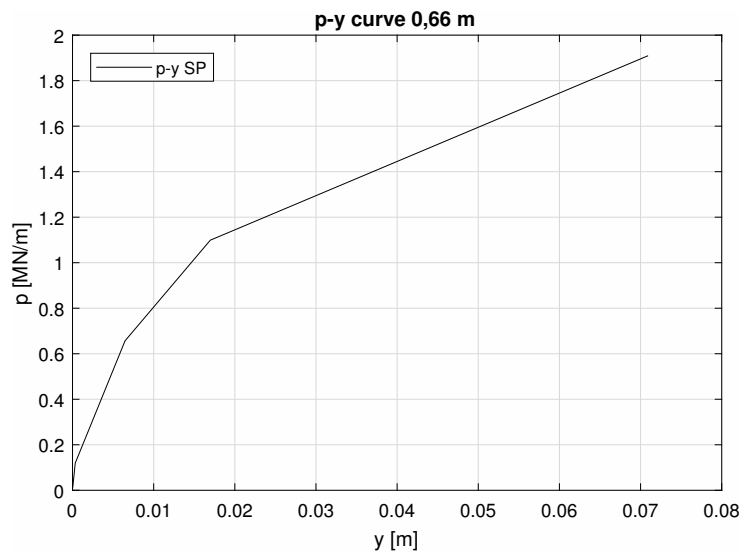


Figure 5.7: p-y curve for SP layer at 0,66 m.

Figure 5.7 shows the p-y curve for the SP layer at 0,66 m height. From the figure it is possible to calculate the stiffness of the layer under different load conditions. The secant stiffness at load step 1000 kN gives a stiffness of around 100 MPa. The stiffness is even higher at lower load steps.

Summary and Conclusion

Offshore wind energy i.e. offshore wind turbines have become a large supplier of clean renewable energy to the European energy market. By the end of 2015 it was installed over 3.200 offshore wind turbines in 84 offshore wind farms in 11 European countries, delivering over 11.000 MW of clean renewable energy to the grid. For offshore wind turbines 80 % of the substructures are monopiles, with an average turbine size of 4,2 MW of output, with average water depth of 27,1 m and 43,3 km from the shore. The trend is an increasing turbine size (14 % larger from 2014 to 2015) and even higher water depth and distance from shore EWEA (2015).

Design principles of large diameter monopiles

The main principle for designing offshore wind turbines with monopile foundation is to fit the natural frequency of the structure within a section of frequencies that is not interfering with the natural frequencies from wind and waves and the rotor and blade passing frequencies. This is done by modelling the pile as beam element with non linear springs, an so called *Winkler foundation* with *p-y* springs. These springs simulate the dynamic response of the soil. The *p-y* approach was originally developed by Matlock (1970) for longer and slender piles used in the oil industry.

The development of the natural frequency of the offshore wind turbine is also dependent of the bed condition over time. When a structure is placed in a marine environment the flow around the structure changes. The structure represents an obstacle that the current or waves (also combined wave and current) have to pass. The presence of the structure can induce wakes and vortexes that increase the shear stress on the bed surface, and when the shear stress is higher than the shear strength ($\tau > \tau_f$) erosion of bed material will start around the pile (scouring). There is different scour conditions where *clear water scour* is the condition where the erosion only happens around the structure and *live bed scour* where the erosion happens over the whole bed. The scour phenomena has been subject to a lot of research and is well understood within smaller diameter structures like bridge piers etc.

Scour can have a substantial impact on the natural frequency of an offshore wind turbine, and with frequency reduction comes possibility of resonance with other prominent dynamic

loads on the structure, this can lead to increased fatigue, shorter operational lifetime and in worst case total breakdown of the structure. To protect a structure from the possibility of scour it is normal to place scour protection around it. The scour protection normally consists of a filter and armour layer consisting of medium and coarse sized stones.

Influence of scour protection on lateral stiffness

The effect of scour protection on the lateral stiffness of monopiles for offshore wind turbines has been investigated through 3D-FEM analysis in Plaxis. The results from the simulations were used to calculate p-y curves for different depths and situations. The results were also compared to the American Petroleum Institute recommended practice for calculating p-y curves for offshore purposes.

The 3D-FEM calculations were done with a model representing a real situation, with real sizes and parameters. The pile was 60 m long with a diameter of 6 m. The pile was embedded 30 m in sand. The sand selected was *Hokksund* sand, a model sand used at NTNU for laboratory tests. Previous testing on this sand done by Sandven (1992); Hanssen (2016) made it possible to obtain parameters for the *Hardening Soil Small* (HSS) soil model to be used in the simulations. The HSS soil model is specially developed to model the soil stiffness in the small strain area, making it perfect for modelling monopiles for offshore wind purposes, as the lateral behaviour is generally in the small strain area.

The FEM simulations was divided into three cases, 1) benchmark case without scour protection, 2) scour protection as surface load and 3) scour protection as a independent layer on top of the subsoil. The reason for making three cases were to have a benchmark to compare the results from the two other cases with, isolate the effect of just the surcharge load on the stiffness of the subsoil and the effect of the scour protection layer on the lateral deflection of the pile. Within these three cases the lateral load was divided in to 5 load steps, 10 kN, 100 kN, 1000 kN, 2000 kN and 5000 kN. The intervals of the load was chosen to give values from both small and larger loads to be able to evaluate the development of the p-y curves. Also the simulation-time increased with the load, and 5000 kN was found to be sufficient when considering the time.

The 3D-FEM model of the soil was divided in to four layers to be able to change the threshold shear strain $\gamma_{0,7}$ in the HSS soil model. Each soil layer was 10 m deep, giving a total soil depth of 40 m. The pile was placed in the middle of the model with 50 m of soil on each side. Only half of the model was simulated, and symmetry boundary condition was used. The pile was modelled with volume elements with equivalent Young's modulus as for a monopile with 80 mm wall thickness. In the middle of the pile a soft beam was placed, from the beam it was possible to extract the bending moment along the pile which then was used to calculate the soil response.

The results from the 3D-FEM simulations show a clear effect of both the surcharge load of the scour protection and the extra layer that the scour represents. The p-y curves from the Plaxis simulations fit well with the p-y curves from the API formulation down to about -3,12 m for the benchmark case, but with larger depths the API formulation predicts higher stiffness than what is observed in the simulations. This is in accordance with findings by among

others Hanssen (2016).

The frequency for the case with only surcharge load is found to be up to 1 % higher for load step of 100 kN than for the benchmark case. For the case with scour protection as a independent layer the frequency was found to be 10 % higher than the benchmark case. This indicates that the scour protection has a substantial impact in the eigenfrequency of a offshore wind turbine, and most impact has the stiff extra layer that the scour protection represents. The stiffness of the scour protection layer was also investigated and was found to be around 100 MPa with the secant stiffness for a load step of 1000 kN, and even higher with lower load steps. This is in accordance with back-calculations of measured eignfrequencies done by Kallehave (2015) where the stiffness of installed scour protection layers around offshore wind turbines was found to be around 200-350 MPa.

The conclusion to this master's project is that the design codes used in the industry for estimating the soil response do not adequately embrace the effect the scour protection has on the lateral behaviour of a monopile foundation. An effect of up to 10 % increase in eigenfrequency is observed when the SP is fully included in the numerical simulations. Both the surcharge component of the SP and the extra layer has an effect. The method used gives a good indication on the effect of the SP, and the observed results fits well with theoretical assumptions and estimation done with the API formulation. Tho the method for extracting the soil response from the 3D-FEM model gives in some cases ambiguous results, specially in the pile rotation point and in the ends of the pile.

6.1 Recommendations for Further Work

This master's project has investigated the effect of SP on the eigenfrequency of offshore wind turbines by conducting a 3D-FEM analysis on a idealised case with parameters from model sand, therefore this model has not been verified or compared against measured values.

- The eigenfrequencies obtained from the model is calculated with a simplified method. The p-y curves should be included in a Winkler model and the eigenfrequency should be calculated and compared to the values found in this thesis.
- The model used in a idealised case with a model sand. The next step would be to apply the method to existing structures to evaluate the procedure and verify results. Some deviation should be expected as the as built/installed properties of a offshore wind turbine could vary from the assumptions done in the design phase.
- In this thesis the soil mechanical behaviour of the SP layer has not been investigated in detail. The SP layer is found to be very important and the behaviour under lateral load should be investigated. The SP is in a crossing between both soil and rock mechanics so both disciplines should be considered.
- The dynamic response of the soil and SP layer has not been investigated. As described in section 2.5 the cyclic loading has an effect on the lateral stiffness of the soil. This degradation should be investigated for both the soil and SP layer. Also the time effect of the soil stiffness degradation should be investigated as measurement done by Kallehave (2015) shows that a drop in eigenfrequency after a storm event (stiffness is degraded) is in most cases temporary. This indicates that the soil regain stiffness over time.

Bibliography

- Achmus, M., Kuo, Y.-S., and Abdel-Rahman, K. (2009). Behaviour of monopile foundations under cyclic lateral load. In *Mathematical problems in engineering*, volume 36. Elsevier.
- API (2011). *API RP2 GEO: Specific requirements for offshore structures, geotechnical and foundation design considerations*. American Petroleum Institute.
- Benz, T. (2007). *Small-strain stiffness of soil and its numerical consequences*. PhD thesis, University in Stuttgart.
- Byrne, B. (2011). Foundation design for offshore wind turbines.
- Centen, I. H. (2015). Predicting scour around offshore wind turbines using soft computing techniques. Master's thesis, Norwegian University of Science and Technology.
- DFI (2013). P-y curves: definition. <http://www.findapile.com/p-y-curves/definition>. Accessed:15.11.2016.
- DNV (2014). *DNV-OS-J101: Design of Offshore Wind Turbine Structures*. Det Norske Veritas.
- EWEA (2014). The european offshore wind industry-key trends and statistics 2015. Report, European Wind Energy Assosiation.
- EWEA (2015). The european offshore wind industry-key trends and statistics 2015. Report, European Wind Energy Assosiation.
- FHWA (2010). *FHWA-NHI-10-016 Drilled Shafts: Construction Procedures and LRFD Design Methods*. Federal Highway Administration.
- Hanssen, S. B. (2016). *Response of Laterally Loaded Monopiles*. PhD thesis, Norwegian University of Science and Technology.
- Hoffmans, G. and Varheij, H. (1997). *Scour manual*. A.A.Balkema.
- ISO (2007). ISO 19902:2007 Petroleum and natural gas industries - fixed steel offshore structures. Technical report, International Standard Organisation. International standard.
- Kallehave, D. (2015). *Monopiles for offshore wind turbines*. PhD thesis, Technical University of Denmark.
- Kim, K., Nam, B. H., and Youn, H. (2015). Effect of cyclic loading on the lateral behaviour of offshore monopiles using the strain wedge model. In *Mathematical problems in engineering*, volume 2015. Hindawi publishing corporation.

- Lombardi, D., Bhattacharya, S., and MuirWoodc, D. (2013). Dynamic soil–structureinteractionofmonopilesupportedwindturbinesin cohesive soil. *Soil Dynamics and Earthquake Engineering*, 49.
- Matlock, H. (1970). Correlation for design for laterally loaded piles in soft clay. In *Offshore technology conference*.
- Moen, T. I. (1978). Hokksund sand. Determination of the sand's routine data, deformation and strength characteristics. Technical Report F78.04, NTH.
- Plaxis (2016). *Material Models Manual*.
- Rocscience (2016). *Manual for RSPile, Laterally loaded piles chapter*.
- Sandven, R. (1992). Hokksund model test sand. Laboratory investigations of index-, strength and deformation properties. Technical report, NTH.
- Stevens, J. and Audibert, J. (1979). Re-examination of p-y curve formulations. In *Offshore technology conference, Huston, USA*.
- Sumer, B. M. and Fredsøe, J. (2005). *The mechanics of scour in the marine environment*. World Scientific.

Determination of HSS Parameters for Hokksund Sand

The sand properties used in the FEM simulations is based on Hokksund sand which is a model sand used in laboratory tests at NTNU. The sand is a uniform, medium grained quartz sand from a natural deposit in Hokksund (Norway). The simulations is done in FEM software Plaxis 3D with *Hardeing Soil Small* (HSS) soil model, a soil model included in the software. The HSS model is a modification of the original HS model, specially developed to capture development of small strains (10^{-6} - 10^{-5}) and small strain stiffness. The HSS model was developed by Thomas Benz at University in Stuttgart and the full description of the model is described in (Plaxis, 2016).

Table A.1: Key soil parameters of Hokksund sand, after Hanssen (2016).

Parameter	Unit	Value
Internal friction angle	[°]	38
Porosity (n)	[%]	39,9
Min. porosity (n_{min})	[%]	36,4
Max. porosity (n_{max})	[%]	48,8
Relative density (Dr)	[%]	76
Density (γ)	[kN/m ³]	16,0
Specific density (γ_s)	[kN/m ³]	27,1
Coefficient of uniformity (C_u)	[-]	2,04
Mean grain size (d_{50})	[mm]	0,38

Hokksund sand is a sand used in model experiments at NTNU and has been subject to many investigations over the years. The soil parameters used in this simulations has been determined by Moen (1978); Sandven (1992) and is summarised in table A.1.

The oedometer stiffness can be described by the Janbu equation for stress dependent stiffness:

$$M_s = m \cdot \sigma_a \left(\frac{\sigma'}{\sigma_a} \right)^{1-\alpha}$$

Where:

M_s : constraints modulus of the soil

m : modulus number

σ_a : reference stress, 100 kPa

σ' : effective vertical stress

α : stress exponent

Oedometer test done by Sandven (1992) found that the constraint modulus of the soil $m = 500$ and Possion's ratio is assumed to be $\nu = 0,2$. The Young's modulus of the sand can then be determined by:

$$E_s = M_s \cdot \frac{(1 + \nu)(1 - 2\nu)}{(1 - \nu)}$$

Where:

E_s : Young's modulus

ν : Possion's ratio

For the HSS model there is a need for more soil parameters, $E_{s,50}^{ref}$, $M_{s,50}^{ref}$, $E_{s,ur}^{ref}$, $G_{s,50}^{ref}$ and $\gamma_{0,7}$. The parameters are given for a reference pressure of -100 kPa (compression is negative in HSS) with the following equations:

$$E_s = E_{s,50}^{ref} \left(\frac{c \cos \varphi - \sigma'_3 \sin \varphi}{c \cos \varphi + p_{ref} \sin \varphi} \right)^m$$

$$G_{s,max} = G_{s,max}^{ref} \left(\frac{c \cos \varphi - \sigma'_3 \sin \varphi}{c \cos \varphi + p_{ref} \sin \varphi} \right)^m$$

$$M_s = M_{s,50}^{ref} \left(\frac{c \cos \varphi - \frac{\sigma'_3}{K_o^{nc}} \sin \varphi}{c \cos \varphi + p_{ref} \sin \varphi} \right)^m$$

Calculation of $G_{s,50}^{ref}$ and $\gamma_{0,7}$

$G_{s,50}^{ref}$ is selected to fit the results from shear wave velocity measurements (G_{max}) done by Hanssen (2016), but for a depth of 40 m. To get a reasonable fit between the SVW measurements and the parameters used in this simulation, c and m in eq. A - A was varied. A cohesion of 1 kPa and exponent m of 0,38 gave a good fit. The equation for $G_{s,max}$ from HSS documentation is:

$$G_{s,max} = G_{s,max}^{ref} \left(\frac{c \cos \varphi - \sigma'_3 \sin \varphi}{c \cos \varphi + p_{ref} \sin \varphi} \right)^m$$

From the results from the shear-wave velocity measurements Hanssen (2016) fitted an equation:

$$G_s = 1000(p_{ref} \cdot \sigma'_v)^{0,5} + 39.000$$

When determining the $G_{s,50}^{ref}$ value the reference pressure is 100 kPa. That gives a G_s value of:

$$G_s = 1000(100 \cdot 100)^{0,5} + 39.000$$

$$G_s = 139.000 \text{ kPa} = \underline{139 \text{ MPa}}$$

Then $G_{s,50}^{ref}$ can be calculated:

$$139.000 = G_{s,max}^{ref} \left(\frac{1 \cos 38 - (-100(1 - \sin 38)) \sin 38}{1 \cos 38 + 100 \sin 38} \right)^{0,38}$$

$$G_{s,max}^{ref} = \frac{139.000}{0,701}$$

$$G_{s,max}^{ref} = 198.571,4 \text{ kPa} = \underline{198,75 \text{ MPa}}$$

The threshold shear strain, $\gamma_{0,7}$, can be calculated with the following equation:

$$\gamma_{0,7} = \frac{1}{9 \cdot G_{s,max}} \left[2c(1 + \cos(2\varphi)) + \sigma'_1(1 + K_0) \sin(2\varphi) \right]$$

The calculated G_0 , $G_{0,HS}$ and γ_{07} with depth is presented in figure A.1. Here $m = 0,38$ and $c = 1,0 \text{ kPa}$ is chosen to give a reasonable fit with the shear stiffness from the shear wave velocity measurements. The fit was favouring the upper layers (>15 m) as they have most influence on the lateral movements of the monopile.

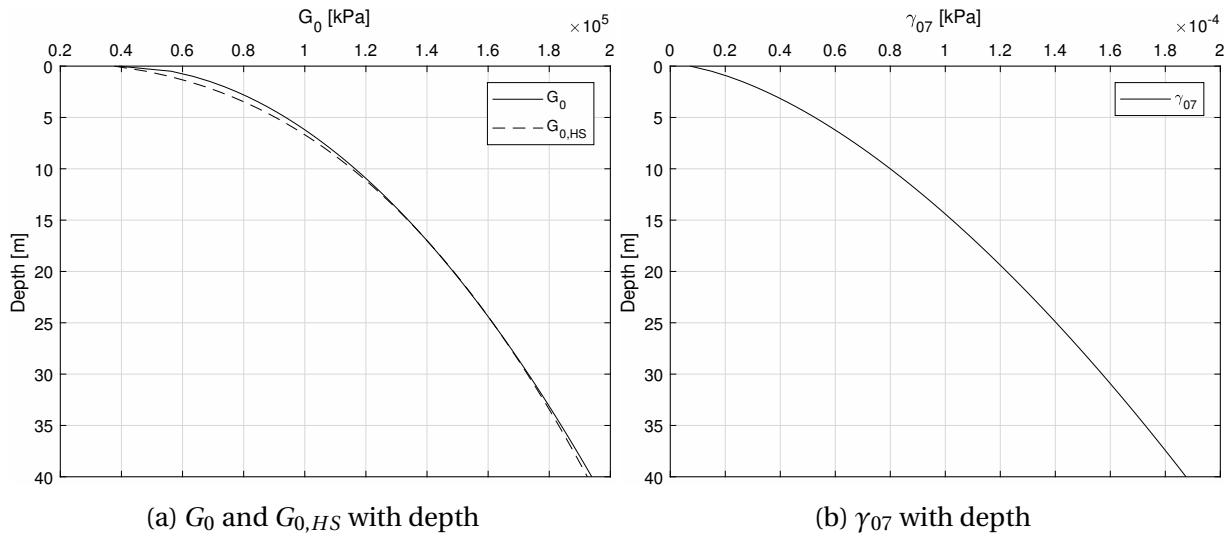


Figure A.1: Change in G_0 , $G_{0,HS}$ and γ_{07} with depth down to 40 m.

Calculation of $M_{s,50}^{ref}$

The reference constraint modulus $M_{s,50}^{ref}$ can be found by introducing a reference stress of -100 kPa in the equation for HSS constraint modulus, where:

$$K_0 = 1 - \sin(\varphi)$$

And

$$\sigma'_3 = \sigma'_1 \cdot K_0$$

The value of M_s is set to be equal to the value from Janbu's formulation at reference pressure (100 kPa):

$$M_s = 500 \cdot 100 \left(\frac{100}{100} \right)^{0,5} = 50.000 \text{ kPa} = \underline{50 \text{ MPa}}$$

When using this in the HSS formulation for modulus number:

$$M_s = M_{s,50}^{ref} \left(\frac{c \cos \varphi - \frac{\sigma'_3}{K_o^{nc}} \sin \varphi}{c \cos \varphi + p_{ref} \sin \varphi} \right)^m$$

$$50.000 = M_{s,50}^{ref} \left(\frac{1,0 \cos 38 - (-100) \sin 38}{1,0 \cos 38 + 100 \sin 38} \right)^{0,38}$$

$$M_{s,50}^{ref} = \frac{50.000 \text{ kPa}}{1}$$

$$M_{s,50}^{ref} = 50.000 \text{ kPa} = \underline{50 \text{ MPa}}$$

Calculation of $E_{s,50}^{ref}$

The reference Young's modulus in HSS is set to be the same as from the oedometer, where the oedometer stiffness is given as:

$$E_s = M_s \cdot \frac{(1 + \nu)(1 - 2\nu)}{(1 - \nu)}, \quad M_s = 50.000 \text{ kPa}$$

$$E_s = 50.000 \cdot \frac{(1 + 0,2)(1 - 2 \cdot 0,2)}{(1 - 0,2)} = 45.000 \text{ kPa} = \underline{45 \text{ MPa}}$$

E_s is then used to calculate $E_{s,50}^{ref}$:

$$E_s = E_{s,50}^{ref} \left(\frac{c \cos \varphi - \sigma'_3 \sin \varphi}{c \cos \varphi + p_{ref} \sin \varphi} \right)^m$$

$$45.000 = E_{s,50}^{ref} \left(\frac{1,0 \cos(38) - (-100 \cdot (1 - \sin(38))) \sin(38)}{1,0 \cos(38) + 100 \sin(38)} \right)^{0,38}$$

$$45.000 = E_{s,50}^{ref} \cdot 0,701$$

$$E_{s,50}^{ref} = 64.194 \text{ kPa} = \underline{64,2 \text{ MPa}}$$